International Journal of Hydrogen Energy 138 (2025) 129–150

Contents lists available at ScienceDirect

International Journal of Hydrogen Energy

journal homepage: www.elsevier.com/locate/he

Computational study of injector cap design for optimized mixing and combustion in a high-performance DI hydrogen engine

Sebastiano Breda [a,*], Veronica Patrizi [a], Fabio Berni [a], Roberto Tonelli [b], Fabio Santi Mortellaro [b], Stefano Fontanesi [a]

[a] University of Modena and Reggio Emilia, Department of Engineering "Enzo Ferrari", Via Pietro Vivarelli 10, 41125, Modena, Italy
[b] Ferrari SPA, Via Abetone Inferiore, 4, 41053, Maranello, MO, Italy

ARTICLE INFO

Handling Editor: Dr C O Colpan

ABSTRACT

At high engine speeds, the reduced time available for fuel–air mixing makes charge preparation a critical factor in optimizing combustion performance and emissions in direct-injection high-performance hydrogen engines (DI H_2-ICEs). Delaying injection into the compression stroke can help mitigate volumetric efficiency losses and reduce the risk of pre-ignition at high loads. However, achieving a sufficiently homogeneous mixture remains essential for stable and efficient combustion. The use of a multi-hole injector cap presents a promising solution, allowing control over jet orientation within the combustion chamber without redesigning the injector body. Nevertheless, the complex interactions between gas jets, in-cylinder flow structures, and turbulence must be thoroughly understood.

This study numerically evaluates the impact of eight different injector cap designs on mixture formation and combustion in a single-cylinder H_2-ICE operating at 6000 rpm, high load (>25 bar IMEP), and at stoichiometry. It presents a novel systematic analysis, considering the pent-roof tumble-based combustion chamber, high-revving and stoichiometric operation. The simulations provide injector design guidelines, revealing that injection along the cylinder axis or in favour of the main tumble vortex improves mixture uniformity by up to 5 %, whereas injecting upstream reduces uniformity by 15 %. The best-performing design achieves a 5 % increase in engine output and a 30 % reduction in combustion duration, demonstrating the effectiveness of optimized injector configuration in improving mixing and turbulence.

1. Introduction

Growing concerns about environmental pollution have led to increasingly stringent regulations aimed at reducing greenhouse gas (*GHG*) emissions. An example is the European Green Deal [1], a comprehensive set of policies shared from EU countries with the final goal of climate neutrality by 2050. According to the European Environmental Agency (EEA) [2], road vehicles are responsible for the 76 % of the transport sector emissions, highlighting the urgent need for accelerated efforts in developing new technologies to drive a rapid decarbonization in transportation.

Electrification is a key strategy, endorsed by legislation, to meet this ambitious goal. However, the transition to fully electrified mobility is proving to be more challenging and time-consuming than expected. This makes the development of zero-emission propulsion systems based on the existing technologies, such as the internal combustion engine, even more strategic. In this regard, carbon-neutral fuels such as bio-fuels and e-fuels can help in the near future to reduce emissions by internal combustion engines. Among the possibilities, hydrogen-based propulsion systems are promising to zero carbon monoxide and carbon dioxide emissions [3].

Green-hydrogen is particularly appealing as an energy carrier for the transportation sector. It can be stored more easily than electric energy, delivered without overloading the grid and flexibly utilized thanks to its peculiar properties. Then, in addition to be fuel for Internal Combustion Engines (*H_2-ICE*) in Hybrid Electric Vehicles (*HEVs*), hydrogen can power fully electrified Fuel Cells Electric Vehicles (*FCEVs*).

FCEVs must face significant market challenges due to their high cost and complexity, but they have the potential to provide fully electric mobility without the range anxiety associated to Battery Electric Vehicles (*BEVs*). Conversely, hybrid power units equipped with *H_2-ICE* exploit the well-consolidated engine technology, offering lower

* Corresponding author.
E-mail address: sebastiano.breda@unimore.it (S. Breda).

https://doi.org/10.1016/j.ijhydene.2025.05.085
Received 23 January 2025; Received in revised form 5 May 2025; Accepted 7 May 2025
Available online 15 May 2025

complexity and maintenance costs. This makes the *HEVs* based on H_2-*ICE* a viable option for accelerating the decarbonization process while addressing current technological and market constraints.

The latter are even more critical when considering specific applications such as high-performance sports cars. Although the overall emissions from this niche market are negligible on a global scale, European legislation mandates that even these vehicles must achieve zero emissions by 2035. While the performance of electric sports cars continues to improve, they have difficulty to captivate engine-enthusiast customers. As a result, many manufacturers are actively promoting the spread of e-fuels or investing in the development of high-specific-power hydrogen engines as alternatives to meet regulatory requirements while satisfying consumer desires.

Hydrogen as a fuel is promising compared to gasoline. The main advantage is the greater flammability range that allows, along with the remarkably higher laminar flame speed, to operate the engine with extremely lean air-fuel ratios (λ), with benefits on engine efficiency and NO_X emissions. However, the lower ignition energy increases the risk of pre-ignition, knock and backfire [3–6].

The easiest way to deliver hydrogen in a Spark Ignition (*SI*) engine is through a Port Fuel Injection (*PFI*) architecture which is, however, the most critical one for backfire and knock. Moreover, gaseous hydrogen injection in the intake port leads to a strong reduction of the engine volumetric efficiency. This results, despite the higher H_2 energy content per unit mass, in a power deficit of about 15 %–20 % compared to gasoline port injection [7,8]. The high risk knock also prevents the operation at stoichiometric conditions, thus further limiting the H_2-*ICE* performance. In order to overcome the specific power reduction, several strategies such as supercharging and cooled *EGR* systems are proposed in literature [8–13].

Some of the issues related to the *PFI* strategy can be avoided by direct injecting hydrogen inside the cylinder after the intake valve closing, thus minimizing risk of backfire and volumetric efficiency reduction. This makes the Direct Injection (*DI*) the most promising and exploited architecture for high power density applications [14].

While in *PFI* H_2 engines a quasi-homogeneous charge can be reasonably sought in the combustion chamber at the end of the compression stroke, in *DI* ones a mixture stratification is expected, with a strong dependency of the latter on injection timing and injector geometry/location, as already demonstrated by several works [15–19]. In addition, a strong influence between *DI* and cylinder flow motions such as tumble and swirl vortex is attended [20]. For this reason, a deep knowledge of the injection event in the actual engine geometry and operation is mandatory, to properly optimize the mixture formation process.

In literature, several numerical and/or experimental studies characterize the hydrogen/air mixing in H_2 *DI* engines. Among the experimental works, the one by Salazar et al. [21] is meaningful as they use Planar Laser-Induced Fluorescence (*PLIF*), with acetone as a fuel tracer, in an optical engine. They investigate, at motored conditions, the impact on the mixture formation of number/orientation of the nozzles and injector location. Based on the data provided by Salazar, Scarcelli et al. [22] validate a 3D-CFD (Computational Fluid Dynamics) model on different nozzle configurations and injection pressures. More recently, Gao et al. [23] numerically investigate the impact of nozzle diameter and injection timing on mixture formation, flow field and combustion. They obtain that, at ultra-lean conditions, the mixture formation process has a primary role in the subsequent combustion evolution and stability. Similar results are obtained by Gammaidoni et al. [24]. They show a big deterioration of the combustion efficiency at ultra-lean conditions when the injection is delayed, due to an ineffective mixture preparation. However, they also show that improvements of the combustion duration can be obtained, with respect to a fully homogeneous charge, with a proper injection strategy. The big impact of mixture inhomogeneity on the combustion phasing, engine variability and NOx emissions are experimentally assessed also by Piano et al. in a recent study on a heavy-duty H_2-*ICE* [25]. All the studies mentioned above are characterized by low load and engine speed, as well as lean (or ultra-lean) mixture quality.

Laget et al. [26] perform a quite extensive analysis of the engine parameters and they identify the mixture preparation as one of the main challenges for the development of new generation H_2-*ICEs*. Mixture heterogeneities are detected as responsible of increased pre-ignition and knock tendency. NO_x emissions also are strongly influenced by mixture heterogeneities as demonstrated by Sfriso et al. [27]. Different results are proposed by Mortellaro et al. [28], via a combined numerical-experimental activity on a single cylinder high performance engine operated at stoichiometric condition. In this case, delaying the start of injection (*SOI*), volumetric efficiency, flame propagation, as well as knock tendency improve, while hydrogen emissions at the exhaust increase. The above discrepancies are not surprising considering the differences between lean/ultra-lean operations and stoichiometric ones. The reactivity of stoichiometric-to-rich mixtures is higher, thus pre-ignition and/or knock are promoted near hot walls. In this scenario, a reduction of the exposition time by delaying the injection seems to be beneficial. However, the literature available on *DI* H_2 *ICEs* operated at stoichiometry, full load and high revving speed is poor and it does not allow final conclusions.

Stoichiometric operation is particularly attractive in the development of high-performance hydrogen engines, to increase the specific power while reducing complexity and cost of turbo/super-charging systems that would be high in case of lean mixtures. In Ref. [29], Medda et al. carry out a thorough investigation on the main challenges in the design of high-performance hydrogen engines for sport cars. They focus on pre-ignition and NO_x emission mitigation without penalizing the specific power. At stoichiometric condition and 6000 rpm, they achieve a peak power of 140 kW/l by employing port water injection to mitigate pre-ignition and using a Three-Way Catalyst to control the emissions. The high reactivity of the stoichiometric mixture leading to pre-ignition and knock (especially at high load and speed) is found to be the main limiting factor to achieve high power densities.

Optimizing the injection system is a key challenge in the design of H_2-*ICE*, as it must be capable of delivering large volumes of gas in a short period to enable delayed injection strategies. Both high and low injection pressure strategies are allowed but, thanks to lower complexity and cost, low pressure solutions (i.e. in the range 20 ÷ 40 bar) currently represent the most adopted one [30]. Pintle injectors are promising due to the high cross flow section. In fact, the low density of H_2 requires, for the needle, larger seat diameter and higher lift compared to GDI hardware. This type of injector permits an easier engine calibration thanks to both the needle lift curve which is pressure-independent and the possibility to optimize the fuel distribution in the combustion chamber by adding jet caps [31]. An example of the effective application of a single hole jet cap instead of a multi-hole injector to improve the performance of a small-bore dual-fuel hydrogen-diesel engine can be found in the recent literature [32].

A recent work by Scalambro et al. [33] shows by numerical simulations as the hydrogen-air mixing can be effectively improved by optimizing the injection phasing and properly orienting the H_2 jet with respect to the organized cylinder flow motion via an injector cap. Interestingly, an injection coherent with the organized flow motion (namely swirl in the specific case) hinders the hydrogen spread in the cylinder and, consequently, the charge homogeneity. Conversely, by orienting the H_2 jet in the opposite direction with respect to the swirl motion improves the mixing. Similar results are confirmed by a recently published study from Akar and Ozener that shows an improvement of the mixing when swirl vortex intensity is reduced [34]. These studies further confirm the importance of characterizing the interaction between cylinder flow motion and hydrogen jet, especially when existing gasoline or diesel units are converted to hydrogen, where strong organized cylinder flow motions (tumble or swirl) exist.

In a recent study Chen et al. demonstrated trough numerical

simulations the strong influence of injector position and interaction between injected hydrogen and organized flow on mixing, combustion and emissions in a pent roof hydrogen engine at low engine speed [35].

Relevant results have been recently obtained by Mortellaro et al. [36], by equipping a *GDI*-derived Single Cylinder hydrogen Engine (*SCE*) with a novel intake duct able to increase the tumble intensity up to 50 %. The higher turbulence effectively improves the combustion stability with delayed injection, at ultra-lean conditions. An improvement of combustion duration and efficiency is met by orienting the hydrogen jet in favour of the main tumble vortex and mounting a properly designed cap on the pintle injector. The adopted strategy allows to improve the mixture quality near the spark plug and eliminate misfires.

The complex interaction between gas jet, organized flow motion and cylinder geometry is difficult to be extensively characterized by experiments, especially at high revving speed, due to costs and technical constraints. In this scenario, 3D-CFD is a valid alternative to deeply understand trends and define design guidelines to improve the mixture formation process in actual engine geometries. 3D-CFD effectiveness in reproducing experimental outcomes is well demonstrated in literature, both considering under expanded gas jets in quiescent pressure vessels [31,37–39] and hydrogen-air mixing in optically accessible units [22,40,41]. The reliability of combustion simulations is also proved. Widespread methodologies relying on chemistry-based laminar flame speed correlations coupled to flamelet combustion models are shown to be effective at different operating conditions (stoichiometric and lean/ultra-lean) [27,28]. 3D-CFD is also adopted in several studies to assess performance and specific characteristics of hydrogen engines without direct validation of the applied numerical models [24,33,38,42,43].

In the current work, the hydrogen air mixing in a single cylinder high performance hydrogen engine is numerically assessed. With respect to previously published studies, the engine operation is peculiar considering revving speed, engine load (6000 rpm, *IMEP*>24 bar) and stoichiometric mixture. The engine has high-tumble architecture, derived from a turbocharged *GDI* unit, and the H_2 *DI* is employed by a centrally mounted pintle injector [28,31]. The numerical model is validated both for gas injection and combustion evolution on available experimental data. The tested baseline configuration, pintle injector w/o cap, is deeply analysed focusing on the interaction between gas jet, tumble motion and cylinder walls. Then, the validated numerical framework is adopted to test different injector cap configurations and the impact of different mixture stratifications on the combustion evolution is assessed. The goal is to establish standard design guidelines, as independent as possible of specific engine geometry, to address the gap currently present in literature concerning high power density engine conditions and pent-roof architecture.

This study represents a groundbreaking contribution to the scientific literature by addressing a previously almost unexplored area of engine research. While prior studies have primarily focused on lean combustion in low-speed engines, this work uniquely investigates the intricate interaction between injected hydrogen and the tumble vortex, a key phenomenon in spark-ignited engines. For the first time, this interaction is comprehensively analysed by combining advanced numerical design exploration with robust experimental evidence. The adverse effect of intense swirl motion on the hydrogen-air mixing process has been demonstrated in the literature [33,34]. In contrast, the present study evaluates the positive impact of injection aligned with the main tumble vortex in a pent roof engine at high revving speed. The findings not only bridge a critical knowledge gap but also establish innovative guidelines for the development of the injector CAP, paving the way for new advancements in this class of engines.

2. H_2 engine and injector features

The engine geometry belongs to a direct-injection spark-ignition single cylinder engine (*SCE*), derived from a Ferrari high-performance turbocharged V6 *GDI* and properly modified to be operated with hydrogen. The main hardware components as well as injection and aftertreatment strategies adopted in the *SCE* layout are extensively described by Medda et al. [29] and they are here briefly summarized in the following for the sake of completeness. A scheme of the combustion chamber and an image of the tested engine are reported in Fig. 1a) and **1b)**, respectively. The hydrogen injector is centrally mounted, while the spark plug is in between the exhaust valves. The engine operation considered for the current activity is characterized by a revving speed of 6000 rpm, high load and stoichiometric mixture, as reported in Table 1.

The injection system consists of a central-mounted pintle injector, developed by Bosch GmbH for low-pressure direct injection in the 5–40 bar range [30,31]. Measurements and visualizations in quiescent vessel of the gas-jet show a strong dependency of both jet shape and penetration on the injector installation. When the injector position is retracted, the gas jet is guided by the walls, thus resulting in a narrower and more penetrating plume. Conversely, when the retraction is minimal (<2 mm), a wider and less penetrating jet is obtained. Given the non-negligible impact of the jet shape on the mixture formation, as shown by the authors in a previous work [31], the control of the injector retraction with respect to the cylinder head is essential. In the present paper, the retraction is fixed to 1 mm to limit the effect of the walls. In fact, although the injection retraction represents a possible strategy to influence the hydrogen-air mixing, a more flexible way to control the mixture formation orienting the gas jet can be realized using an injector cap, as schematized in Fig. 2. This component is directly mounted on the injector tip and it can be characterized by single- or multi-hole designs, leading to a flexible optimization of the mixing without modifications of the injector design.

In this work, 15 different injector caps are tested, characterized by different number, diameter and orientation of the holes. The final goal is to define design guidelines to improve the mixture homogeneity at the end of the compression stroke with a delayed injection strategy. In the following sections, only the most significant results (obtained with 8 different caps) will be analysed (see Table 2). Moreover, combustion is also simulated for the 4 best performing caps, to study how the reaction progress is affected by the different fuel stratification and turbulence.

3. Numerical model setup and validation

Two different CFD models are developed for the study. The first one is representative of a quiescent vessel and it is adopted to define the numerical setup for the gas injection simulation. The model validation is performed comparing numerical results with experimental data (in terms of penetration, width and shape of the gas jet) on equal operating conditions. The experiments are carried out at Robert Bosch GmbH and details on the applied methodologies are published in Ref. [30]. The methodology defined at this stage is finally applied to the in-cylinder model for the evaluation of the mixing in the actual engine geometry. Hydrogen combustion is also simulated and the relative numerical setup is validated against experimental outcomes of cylinder pressure and combustion indicators. The experiments on the SCE are performed at the powertrain department of Ferrari SPA as described in Refs. [28,29]. All the analyses are performed using STAR-CCM + software in a RANS framework.

3.1. Gas injection model validation

Almost the same setup proposed by Paltrinieri et al. [31] in a previous validation work is adopted. Therefore, only the most significative needle portion of the injector is simulated and, thanks to the geometrical symmetry of the problem, only ¼ of the overall physical domain is considered. The needle opening is not simulated, the poppet valve position is fixed to the maximum measured lift and the time varying measured mass flow rate is applied. A more refined setup including needle lift motion with a pressure condition at the inlet boundary

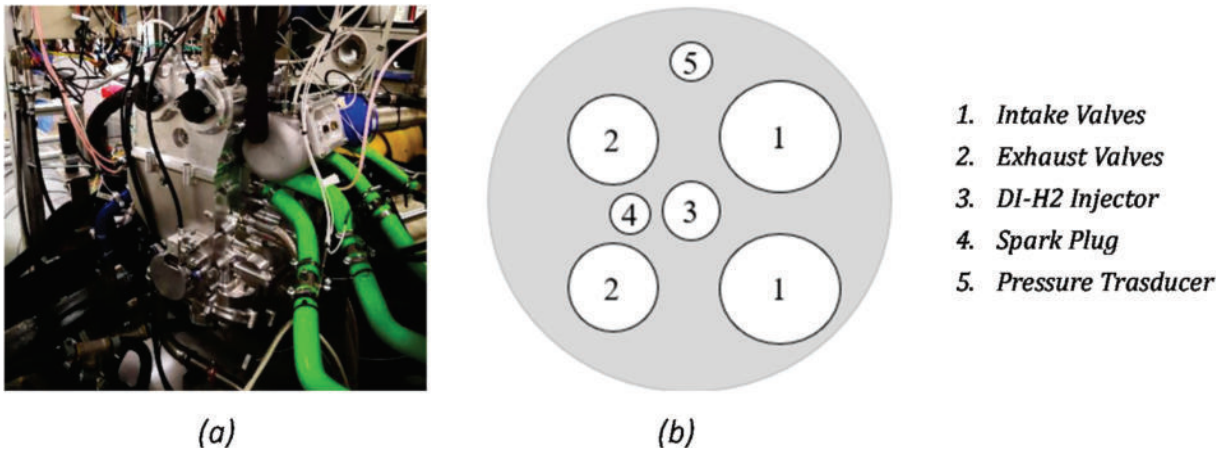

Fig. 1. Analysed engine layout.

Table 1
Engine characteristics and operation.

Single cylinder Engine Operating Conditions	
Bore/Stroke	88/82 mm
Compression ratio	10.5:1
RPM	6000
Load	Wide Open throttle (*WOT*), IMEP>25 bar
Lambda index	1.0 (*Stoichiometric*)
SOI (≈IVC)	140° bTDC (effective value 137° bTDC)
Injection duration	80°
Injector mass flow rate	15 g/s @25barA/85°
Injection pressure	≈40 bar

(instead of a mass flow rate one) would be possible and (probably) more accurate in capturing flow details during the needle opening phase. However, it would lead to extremely higher computational costs, not in line with the final aim of testing several cap configurations. Considering the short duration of the needle opening phase compared to the overall injection event, gas jet shape and penetration can be reasonably captured despite the simplification and, simultaneously, with a big advantage in terms of simulation CPU cost.

The main characteristics of the computational mesh selected for the study are reported in Fig. 3. A maximum cell size of 0.5 mm is selected for the core of the vessel, where the jet evolves, while static refinements are applied in the needle region, reaching a minimum size of 31.25 μm in the poppet valve curtain. Considering the high flow velocity and the fine mesh, a numerical timestep of 2.5×10^{-8} s is adopted, to limit Courant number and, thus, to ensure solution convergence. According to widespread best practices for 3D-CFD in-cylinder simulations [24,28,43], the RNG k-ε model is applied for the mixing and combustion analyses proposed in the present work. Coherently, also in the vessel simulations the same turbulence model is adopted. A two-layer all-y^+ approach is exploited as near wall treatment. The Pressure Implicit with Splitting Operators (*PISO)* algorithm coupled to a second order discretization scheme for energy, turbulence, momentum and species are adopted. Considering the peculiar values of pressure and temperature reached in under-expanded gas jets, temperature dependent gas properties are considered. Moreover, Soave–Redlich–Kwong real gas equation of state [37,44] is adopted instead of the ideal gas formulation. To track the jet, according to the existing literature [37,45–47], a mass fraction iso-surface calculated at 0.05 is considered. As for the penetration, the maximum axial distance of the defined iso-surface from the injector tip is extracted. In addition to the reference configuration, other two cases obtained by increasing and reducing of 1 mm the injector axial position are also simulated for the sake of validation.

The three investigated configurations refer to a different injector retraction with respect to the seat. In the neutral position, i.e. flush mounted injector, the cap is aligned with vessel head, promoting a hollow-cone jet formation. As the retraction increases, the shape significantly changes. At the maximum retraction, the jet becomes straight and highly-penetrating. As anticipated above, the reference for the analysis proposed in the following is the mid-configuration with a retraction (Z) of 1 mm. The main results of the validation activity are reported in Fig. 4. From a global standpoint, the model reasonably reproduces the experimental outcomes. The spray penetration variations with the injector retraction are well captured. Despite some discrepancies, the numerical deviation is lower than 10 % with respect to the experimental counterpart and it mainly involves the middle-final part of the injection event. Fig. 5 presents a comparison of jet evolution images between software-generated iso-surfaces and optical window images obtained from Schlieren analysis for the engine-mounted configuration (Z = 1 mm), highlighting the accuracy of jet evolution detection.

Starting from the reference configuration, a sensitivity study is performed by minimally varying the injector retraction. As reported in Fig. 6, it is observed that, shifting the injector by ±0.025 mm, a non-negligible variation in the jet penetration is obtained. This result is confirmed when a further ±0.2 mm shift is applied. Thanks to the performed sensitivity, it is possible to state that the current configuration is very sensitive to small variations of the retraction. This encourages even more the adoption of an injector cap to avoid undesired effects due to injector position uncertainties.

3.2. In-cylinder model validation

A 3D-CFD in-cylinder model of the actual engine including a portion of intake and exhaust ports and the hydrogen injector tip is built to simulate an engine cycle with injection, mixing and combustion. The symmetry of the engine geometry is exploited, thus only half of the overall fluid domain is considered, to reduce the computational time. Pressure/temperature time-dependent boundary conditions extracted from a validated 1D model of the engine are applied and dedicated temperatures are fixed at the walls of each component. Mesh characteristics and numerical setup of the simulations are defined according to the validation study on the static vessel. As for the mesh, a base size of 1 mm is adopted for cylinder and ports. During the entire injection event, a conical mesh refinement of 0.5 mm is created to ensure that the gas jet evolution occurs in a refined region as the one in the vessel. The same mesh refinements are also adopted for the nozzle tip. With the described mesh setup, the maximum number of cells during the hydrogen injection is about 3.5 million (for half of the combustion chamber). A time step of 0.002° *CAD* (corresponding to 2.78×10^{-8} s at 6000 rpm) is defined during the injection while 0.05 *CAD* is adopted during combustion, thus resulting in a quite expensive computational effort. For completeness,

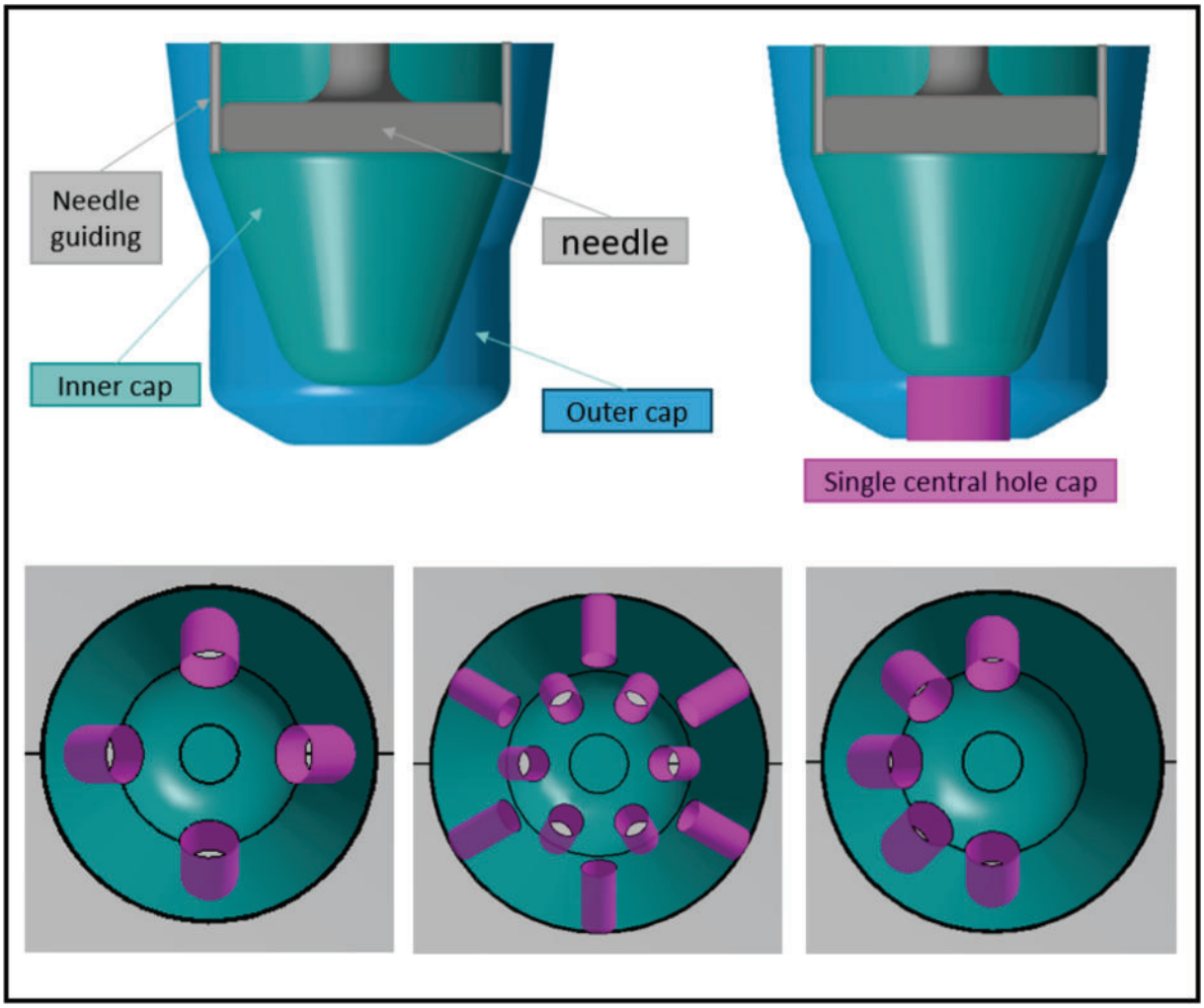

Fig. 2. Injector cap assembly: various examples of cap designs are proposed.

Table 2
Characteristics of the tested injector caps.

Case Name	Holes Number	Holes Diameter [mm]	Description	Radial spacing (°)	Axial spacing (°)
A	1	3.50	Single axial hole	–	0°
B	3	2.02	3 holes exhaust oriented	90°	22°
C	3	2.02	3 holes intake oriented	90°	22°
D	5	1.58	5 holes symmetric	90°	30°
E	5	1.58	5 holes exhaust oriented	45°	22°
F	5	1.58	5 holes exhaust oriented	45°	30°
G	12	1.04	12 holes, single ring	30°	30°
H	12	1.04	12 holes, dual ring	60°	30°/15°

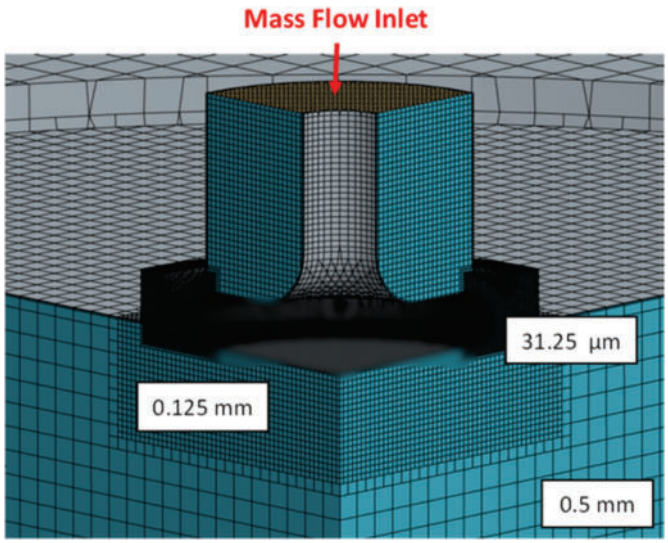

Fig. 3. Computational grid details. Needle geometry is blurred for confidentiality reasons.

almost 100h on 96 *CPUs* are needed for a full engine cycle simulation. Assuming that the in-cylinder flow before the injection is scarcely affected by the injector design (with or without injector cap), a full-cycle simulation is performed only for the baseline case. For the tests of the different the injector caps, simulations start at 140 *CAD bTDC*, i.e. when

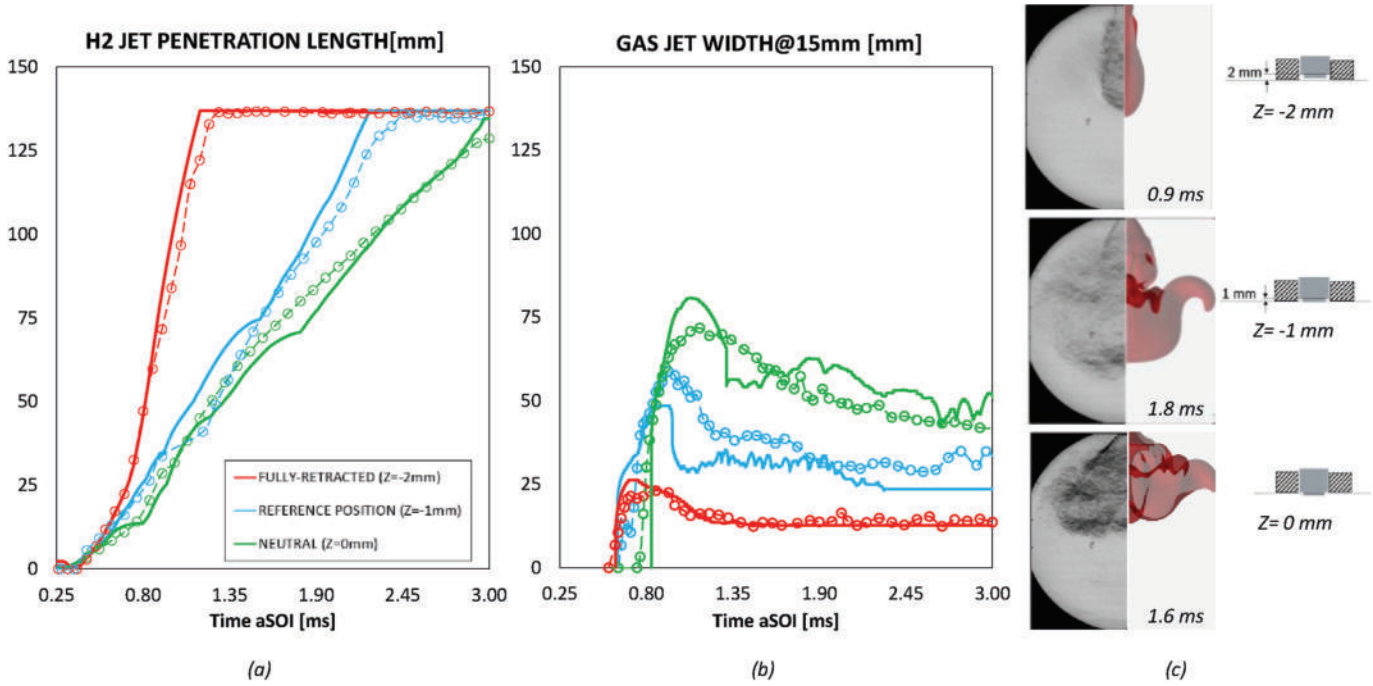

Fig. 4. (a–b) jet penetration and width for different injector retractions. Dotted and continuous lines represent experiments and numerical outcomes, respectively. (c) numerical-experimental comparison in terms of jet evolution.

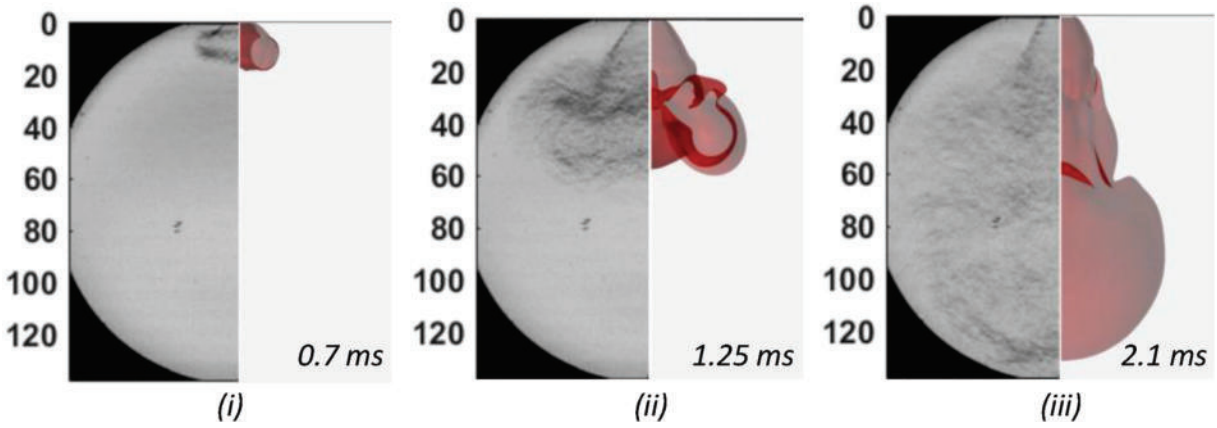

Fig. 5. Visual time-dependent evolution: reference experimental (left) vs. numerical (right) at three different timing.

the valves are already closed, using as initial conditions the fields from the full-cycle simulation carried out on the baseline case. This allows to remove from the model both intake and exhaust ports, saving almost the 20 % of the computational time for each of the simulated designs. An image of the defined engine model is reported in Fig. 7, where the conical mesh refinement defined during the injection is visible.

The Extended Coherent Flame Model (*ECFM-3Z*) [48] is applied for the combustion simulations. This model is extensively adopted and validated in literature for the simulation of turbulent flame propagation in high performance engines, at conditions similar to those investigated in the present work. Moreover, *ECFM-3Z* is validated with both traditional and alternative fuels, including hydrogen [28,43,49,50].The model requires, as an input, Laminar Flame Speed (*LFS*) and Laminar Flame Thickness (*LFT*) of the actual fuel as a function of pressure, unburnt temperature and mixture quality. Therefore, *LFS* and *LFT* tables are generated by 1D chemical kinetics calculations using the DARS CFD chemistry solver. The tables are generated to cover all the possible physical states experienced by the mixture, i.e. pressure, temperature, equivalence ratio and EGR percentage ranges are 10 ÷ 150 bar, 150 ÷ 1250 K, 0.2 ÷ 2.5 and 0 ÷ 30 %, respectively. XJTUNO-2021 mechanism [51] is identified as the most suitable one by literature review and sensitivity studies [52–54]. The ignition process is modelled by the Imposed Stretch Spark Ignition Model (*ISSIM*) [55], which requires as an input some ignition system specifications. The wall heat transfer is calculated by the GruMo-UniMORE model [56–58].

The numerical framework for the combustion simulations is validated comparing CFD results and experimental outcomes on the baseline case (without injector cap). As reported in Fig. 8, cylinder pressure from both experiments and CFD is compared and adopted to calculate apparent heat release rate and combustion durations. The model is able to reliably predict the combustion evolution. Combustion phasing and early combustion duration are almost perfectly matched, while the second half of combustion duration is overpredicted, thus leading to an overestimation of the 10 ÷ 90 % duration of 15 %. Despite some model weaknesses related to the flame-wall interaction when using H_2 as a fuel, the combustion results on the baseline case are considered as robust. In other words, the in-cylinder model can be adopted to assess the impact on the combustion evolution of different injection cap designs (see

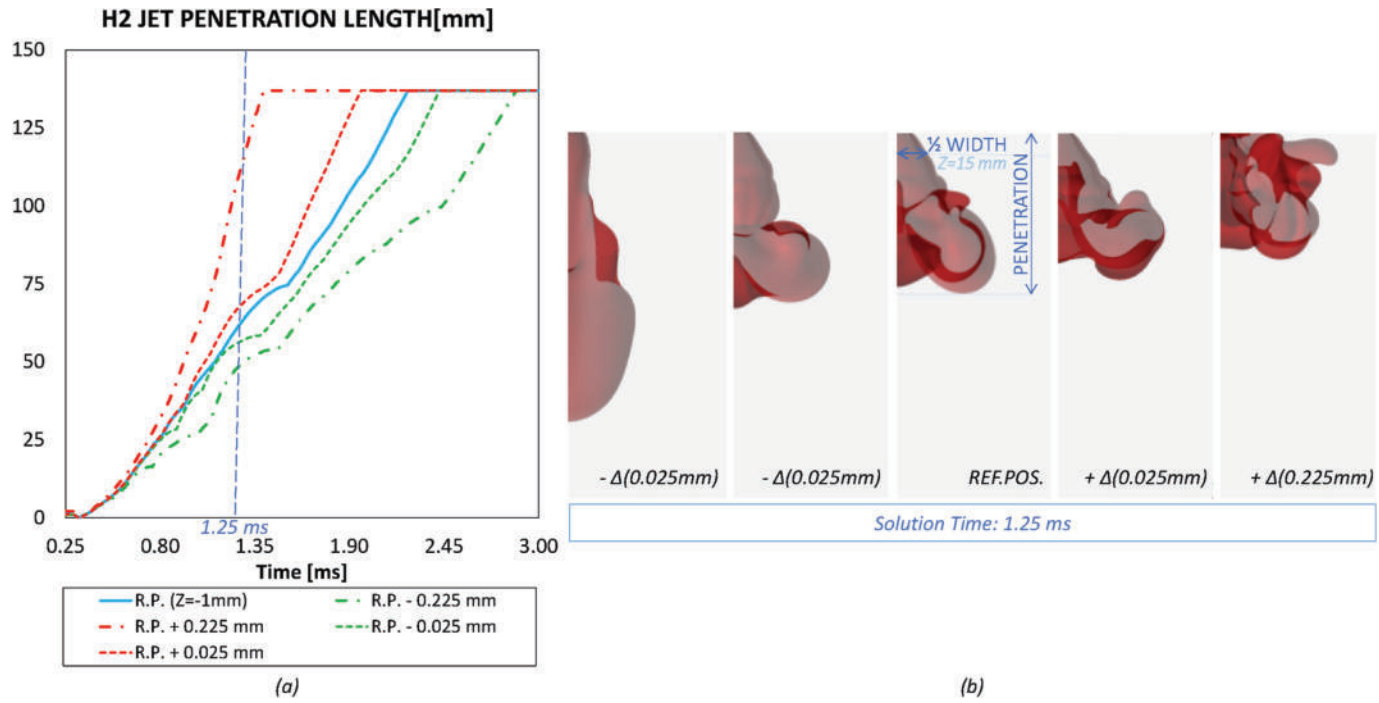

Fig. 6. (a–b) sensitivity analysis of jet penetration and shape to the injector retraction (ref. time = 1.25 ms).

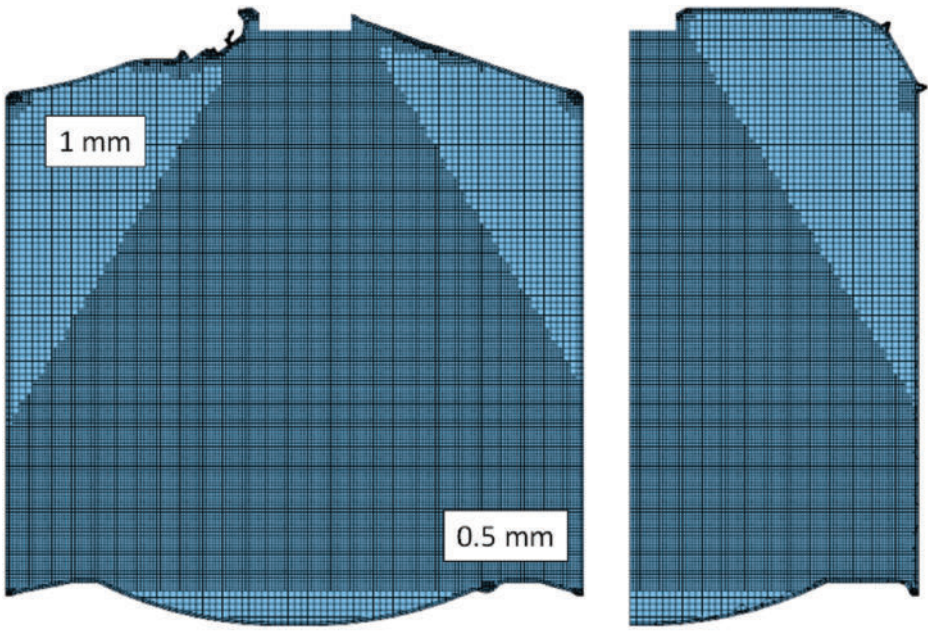

Fig. 7. The computational mesh adopted for the simulations on two orthogonal section planes passing through the cylinder axis. The left image displays the symmetry plane of the combustion chamber, while the right shows the orthogonal plane.

Fig. 9).

4. Discussion and results

In this section, the results of the numerical study will be presented and discussed. Firstly, the mixture formation process in the baseline case (*DI* without injector cap, Z = −1mm) will be deepened, as it is the benchmark configuration for the injector cap development study. In this section, methodology and parameters adopted to evaluate the quality of the mixture in the proposed cases will be also described. Secondly, the mixture formation process when applying 8 different injector cap geometries to the original *DI* injector is discussed.

All the caps are designed to ensure the geometrical symmetry of the combustion chamber. The number and diameter of the holes are case-by-case defined to maintain a slightly larger cross-sectional area compared to the actual poppet valve curtain area. This design approach minimizes pressure drops through the holes while ensuring a moderate pressure rise inside the cap. By doing so, it preserves the assumption of a consistent flow rate profile across different configurations and avoids an unfeasible increase in the required injection pressure for the same mass flow rate boundary condition.

The impact of increased pressure drop on the mass flow rate is

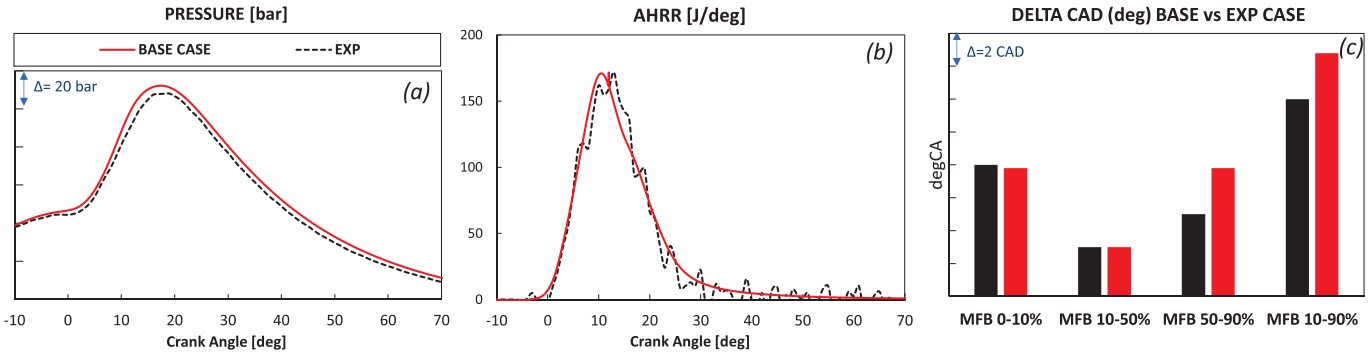

Fig. 8. Experimental vs numerical results in terms of (a) mean in-cylinder pressure, (b) heat release and (c) combustion indicators.

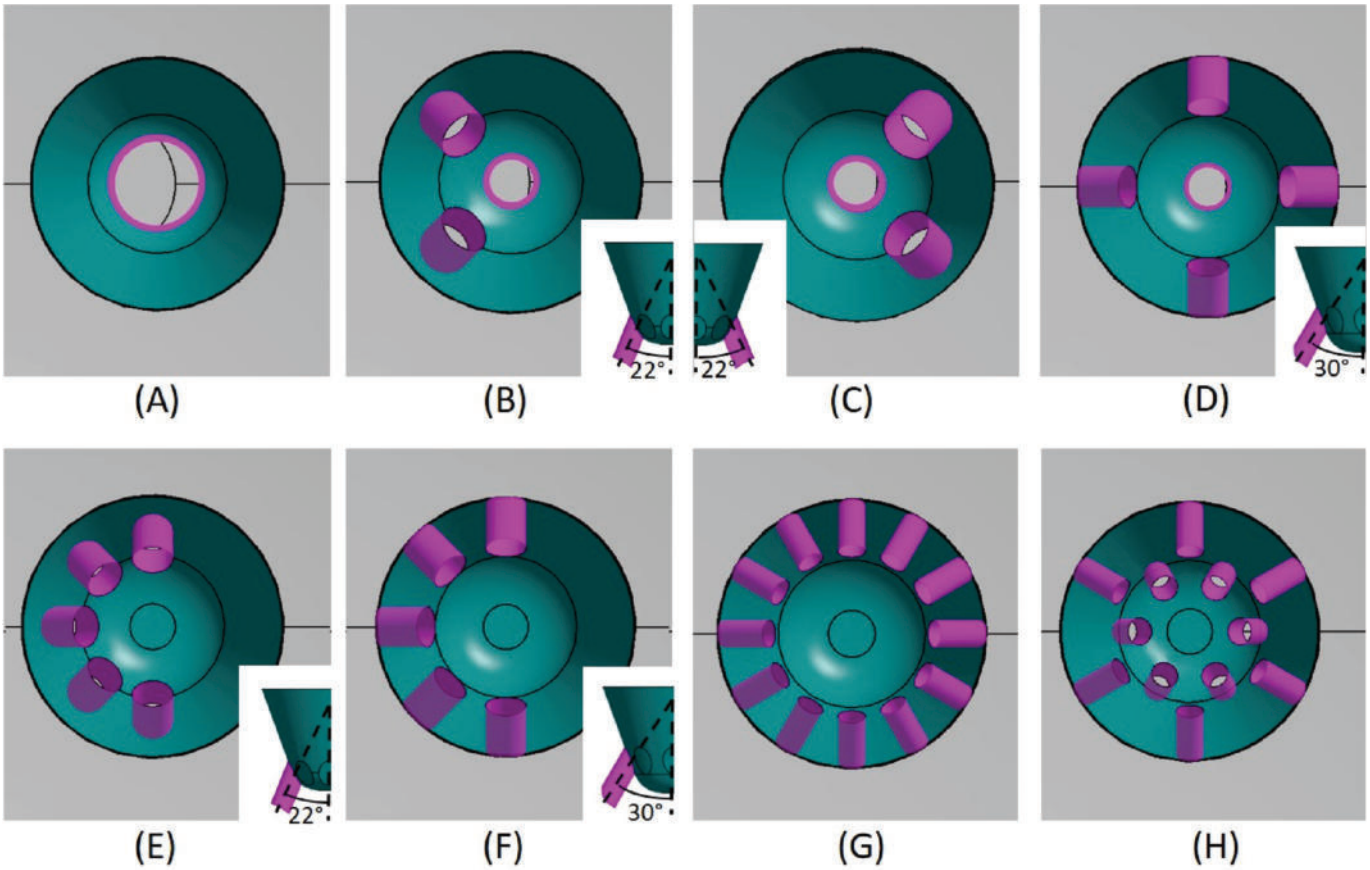

Fig. 9. Injector cap drilling (top view). Cap holes are highlighted in pink color. (For interpretation of the references to color in this figure legend, the reader is referred to the Web version of this article.)

carefully inferred using steady-state simulations in the vessel, applying the baseline injection pressure of 34.8 bar as a boundary condition instead of mass flow rate. The most critical case, represented by the 12-hole cap, shows an 11 % reduction in the calculated mass flow. To compensate, a 12.5 % increase in the injection pressure would be required to achieve the same flow rate of the baseline injector without the cap in the most critical configuration. Fortunately, the injector hardware is specifically designed to handle this pressure increase, ensuring a consistent mass flow rate profile across all cap configurations. This consistency enables a coherent and reliable analysis while retaining identical injection phasing and duration for all scenarios accepting a slight increase of the injection pressure.

The cases are named so that, moving from "A" to "H", the complexity increases. "A" indicates the single hole configuration, while "H" stands for the 12-holes one. A couple of 3-holes designs is considered. One is characterized by holes directing the hydrogen jets towards the exhaust side in favour of the tumble vortex ("B"), while the other has holes facing towards the intake side ("C"). Considering the better results obtained orienting the jets towards the exhaust, two of the three 5-holes configurations are defined with jets directed on the exhaust side ("Ee" and "F"). The comparison between "E" and "F" represents a sensitivity to the hole orientation angle with respect to the cylinder axis. A symmetric 5-holes cap is also tested ("D"). Then, 12-holes configurations are investigated to verify if the uniformity increases by strongly augmenting the number of holes. Globally, four configurations ("A", *"D", "G",* "H") are symmetric with respect to the intake/exhaust sides, while the remaining ones ("B", *"C", "E", "F"*) have a preferential distribution.

In the last section, the combustion evolution for the 4 most promising cases is investigated and compared to the baseline one. Preliminary, for the sake of comparison, the same spark-time of the reference case is

maintained for all the cases. Then, a spark-time sweep is performed to reach with all the cases the same combustion phasing of the baseline one. In this way, a fairer assessment of the combustion performance changing the cap design is possible.

4.1. Baseline case without injector cap

The mixture formation process in the baseline case is here presented and studied, to be used as benchmark configuration to evaluate the performance of the different injector cap designs. The fuel spread in the combustion chamber is tracked visualizing, during the injection phase, the H_2 mass fraction evolution while, at the end of the compression stroke (10 *CAD bTDC*), the Lambda index field is considered. To further deepen and make the charge stratification study quantitative, Probability Density Function (*PDF*) of the Lambda field and Route Mean Square (RMS) of the same quantity are extracted for each case and evaluated. The charge homogeneity is quantified by a volume-based Uniformity Index (*UI*) defined as in Equation (1), where V_c is the volume and λ_c is the lambda index, both for the *i-th* computational cell. The average lambda index $\bar{\lambda}$ is computed as in Equation (2), where *V* is the volume of the combustion chamber

$$UI = 1 - \frac{\sum_V |\lambda_c - \bar{\lambda}|\, V_C}{2\,\bar{\lambda} \sum_V V_c} \quad \text{(Equation 1)}$$

$$\bar{\lambda} = \frac{1}{V} \sum_V \lambda_c V_C \quad \text{(Equation 2)}$$

The maximum value for the *UI* is 1, indicating a perfectly homogeneous mixture. When the mixture inhomogeneity increases, the *UI* reduces. The interaction between hydrogen injection and in-cylinder flow as well as the turbulence generation are also analysed by Tumble Ratio (*TR*) index and Turbulent Kinetic Energy (*TKE*). The TR is defined in Equation (3) as the ratio between the fluid angular momentum referred to the cylinder centre of mass and the engine rotation speed. In Equation (3), L_T is the angular momentum, I_T is the moment of inertia of the fluid with respect to the tumble axis and N is the rotational speed of the engine expressed in rpm. The reference is a right-handed cartesian coordinate system with x-axis pointing to the intake side and z-axis directed upward. The tumble axis is directed as the y-axis of the same coordinate system. With respect to the above reference, the typical tumble vortex generated by the flow through the intake valves results in a negative *TR* index, that becomes even lower when the tumble vortex intensity increases.

$$TR = \frac{L_T / I_T}{2\pi N / 60} \quad \text{(Equation 3)}$$

The interaction between bulk flow, turbulence and hydrogen injection in the baseline configuration is analysed simulating an overall engine cycle, with and without fuel injection. Tumble vortex intensity as well as turbulence evolution are monitored and reported in Fig. 10. The gas fuel injection negatively affects the tumble vortex that dissipates earlier with respect to the reference case without injection, reaching an almost zero *TR* value at the end of the compression stroke. This is related to the creation of a counterrotating vortex from the interaction of the hydrogen jet with the piston crown as it will be further deepened in the following. Regarding the turbulent kinetic energy, direct injection strongly enhances the turbulence level inside the cylinder, but the jet induced turbulence dissipates quickly leading to a residual turbulence level at the compression stroke end that is like the one without fuel injection. The interaction between incoming gas jet, bulk flow and turbulence are considered in the following, when jet orientation and velocity are modified by the introduction of an injector cap. In particular, the enhancement of the *TR* thanks to the injection can promote the increase of the turbulence level during combustion, with beneficial effects in terms of efficiency and duration.

Fig. 11 shows the evolution of the hydrogen jet during injection for the baseline case, visualized on two orthogonal section planes passing through the cylinder axis, including the combustion chamber symmetry plane. As visible from the previous validation study, a quite widespread jet is detected 20 *CAD aSOI* due to the intermediate injector retraction. Nonetheless, the high axial momentum of the gas-jet overtakes the in-cylinder bulk gas motion effect, with an almost negligible deviation of the gas jet until 60 *CAD aSOI*. Hydrogen fast penetrates thanks to low chamber back pressure and intermediate injector retraction. Then, it strongly impinges the piston crown moving upwards and it creates two counter-rotating wall-guided vortices. The latter are not fully symmetric as the counterclockwise vortex (on the intake side) is more intense. This can be explained with both the slight asymmetric piston bowl and majorly due to the vortex amplification by the tumble motion. When the injection ends (80 *CAD aSOI*), the interaction between bulk flow and hydrogen jet becomes even more predominant and it is the main mechanism responsible for the fuel spread in the combustion chamber. The described interaction between cylinder walls, gas jet and bulk flow accumulates hydrogen in the periphery of the combustion chamber, mainly on the intake side. A lean combustion chamber core is obtained, as visible analysing the Lambda distribution at 10 *CAD bTDC* reported in Fig. 12. A very lean mixture pocket is also observed in the periphery of

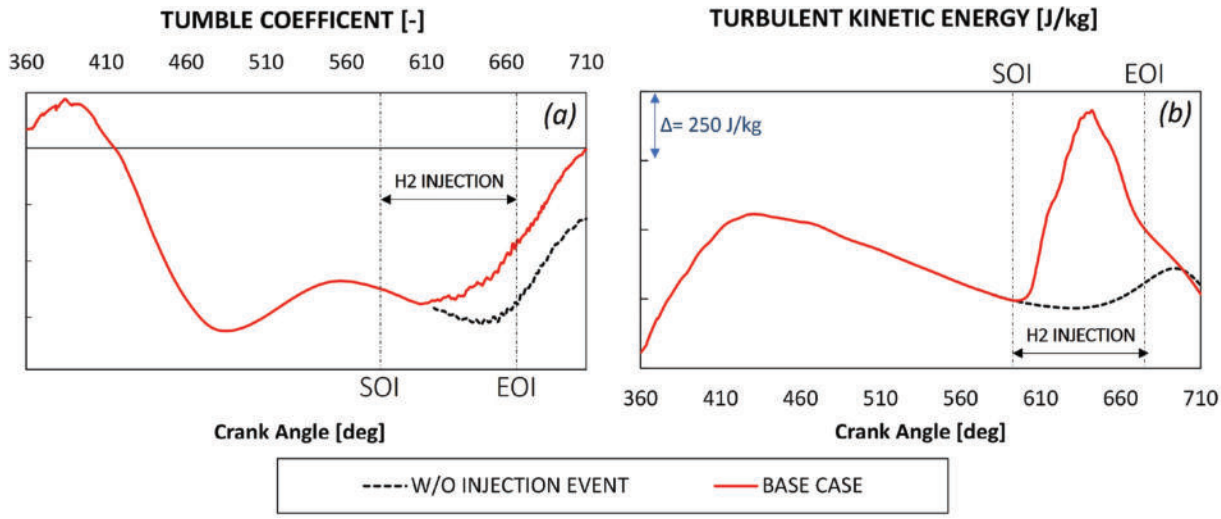

Fig. 10. Tumble ratio (a) and Turbulent kinetic energy (b) evolution during intake and compression strokes (360 deg = TDC).

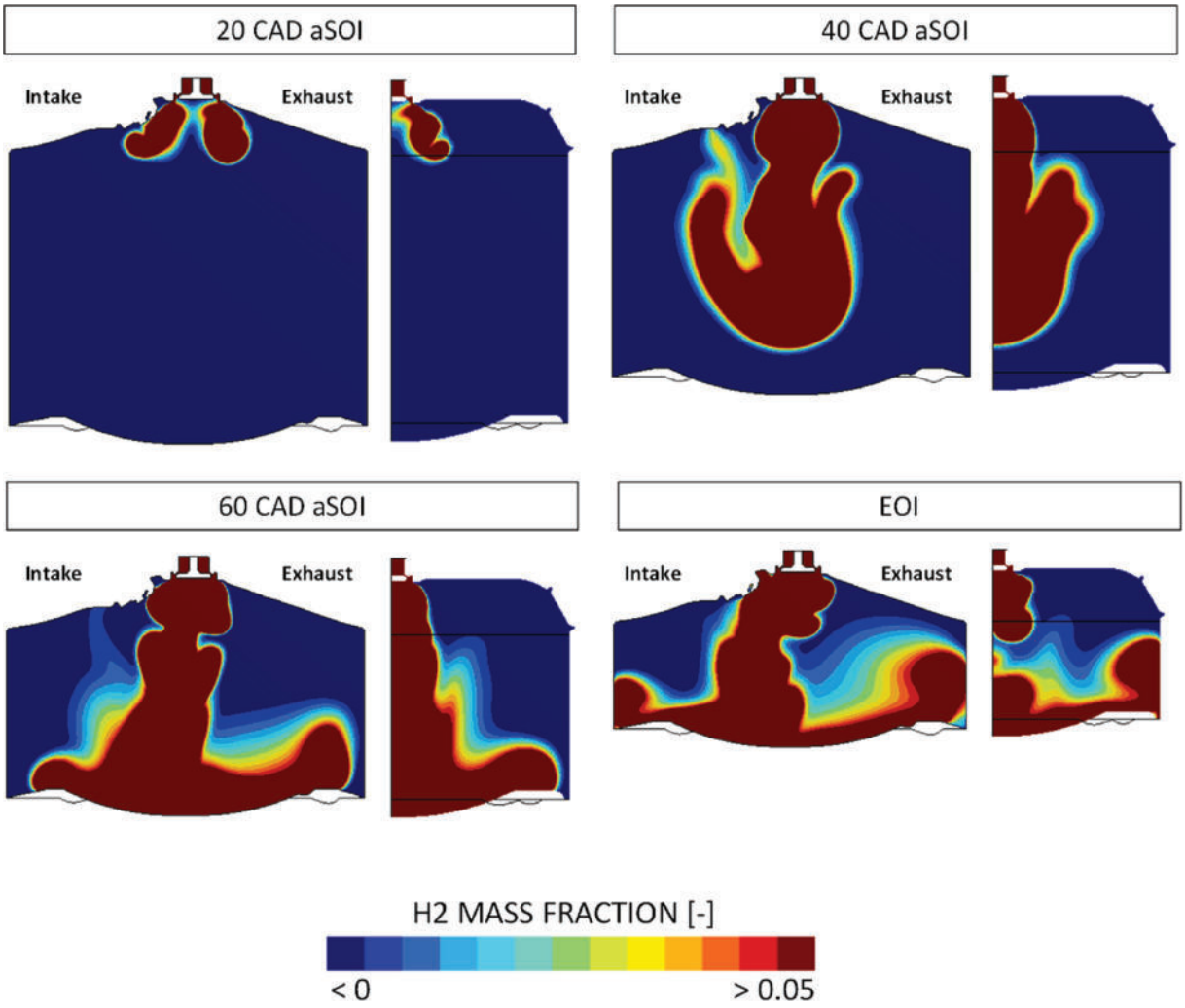

Fig. 11. H_2 jet evolution in the baseline configuration on two orthogonal section planes intersecting the cylinder axis. The left image shows the symmetry plane of the combustion chamber, while the right image presents the orthogonal plane.

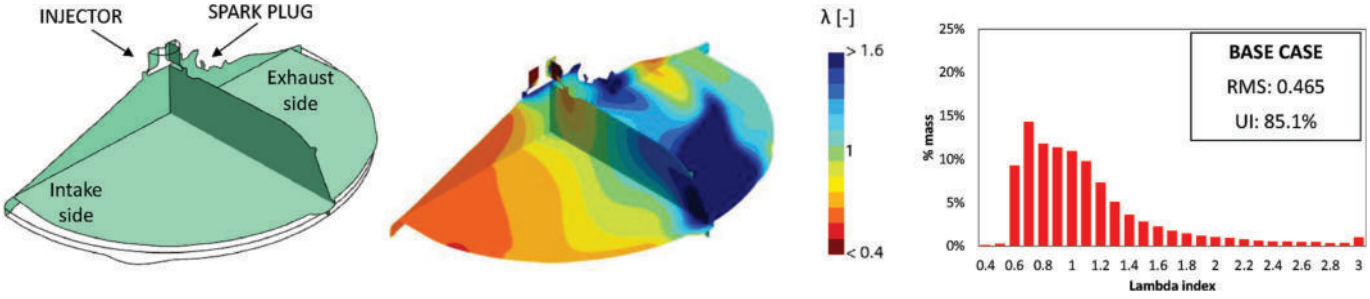

Fig. 12. Baseline case stratification analysis in terms of in-cylinder lambda index distribution and related probability density function.

the combustion chamber. The *PDF* of Lambda is also reported in Fig. 12, showing a quite spread distribution and, thus, the non-negligible presence of wide regions characterized by mixtures far from being stoichiometric. The standard deviation of the Lambda field is therefore high and equal to 0.465, while the resulting *UI* is 85.1 %. Close to the spark electrodes, a lean mixture is created (λ is 1.26 on average).

4.2. Mixing analysis with different injector cap designs

In the current section, the mixture formation process when applying different injector caps is studied. Firstly, the application of a single hole axial cap is compared to the baseline configuration. Secondly, multi-hole setups are considered. Sensitivities to jet orientation and distribution are performed, with a focus on the interaction between gas jets, bulk flow and cylinder walls.

4.2.1. Case "A": single-hole cap

The impact on the mixture formation when adopting a single hole cap is presented in the following. The evolution of the jet resulting from the single-hole cap can be found in Appendix 1. With respect to the baseline case, and similarly to what happens when retracting the injector position, a higher jet penetration is obtained. This is due to a

narrower gas jet that favours a higher jet momentum along the vertical axis. Almost no deviation of the jet by the bulk flow is noticed till the end of the injection. Similarly to the baseline case, two counter rotating (but stronger) vortices are created when the jet impacts the piston crown. The tumble motion helps in moving the hydrogen at first towards the intake side and, after, towards the exhaust one, following the combustion chamber walls. Still in comparison with the baseline case, the final result is a more symmetric fuel stratification characterized by rich mixture on both intake and exhaust peripheries and a leaner one in the combustion chamber core, as visible from Fig. 13. The lean mixture pocket in the periphery of the combustion chamber visible in Fig. 12 is still noticeable but reduced. Similarly, also the chamber portion characterized by λ higher than 3 decreases.

Despite the narrower jet during the injection, the charge homogeneity at the end of the compression stroke globally improves, as quantitatively confirmed by the narrower *PDF* of the Lambda index, the lower Lambda *RMS* (which reduces to 0.376, i.e. −19 % with respect to baseline case) and the increase of the *UI* from 85.1 % to 87.5 %. The mixture quality near the spark electrodes improves as well, reaching a quasi-optimal condition (λ = 0.84). The increase of the tumble vortex dissipation noticed in the baseline case is not found when the single-hole cap is adopted. Conversely, the tumble vortex intensity is enhanced by the gas jet. The injection-induced turbulence increases, thus resulting in a higher turbulence at the end of the compression stroke (of nearly 30 % on average), thanks to the enhancement of the main tumble vortex that better resist to the energy cascade process. The evolution of both *TR* and *TKE* with the single hole cap is reported in Fig. 14.

From both mixing and flow standpoint, case "A" behaves better than the baseline one, confirming the beneficial effect of the adoption of an injector cap, even if no preferential direction to the incoming gas jet is imposed by the cap. Furthermore, the maximization of the jet vertical momentum that increases the interaction between injected hydrogen and piston crown is beneficial by improving the fuel spread in the combustion chamber. Generally, the interaction between gas jet and cylinder walls has a primary role on the final mixture stratification.

4.2.2. Cases "B" and "C": 3-holes caps

In this section, the results obtained with 3-holes injector caps are analysed. Case "B" is characterized by holes injecting towards the exhaust side, while case "C" is perfectly specular to the previous one, i.e. jets are directed to the intake. Considering the air coming from the intake ports and directed towards the exhaust side to generate tumble, the injection occurs in favour of the main tumble vortex in case "B", while it is against the same in Case "C". The 3-holes configurations present a central vertical hole, which is maintained compared to case "a" considering the positive impact on mixing and turbulence as shown in the previous section. The evolution of the hydrogen mass fraction during injection and compression stroke is reported in Appendix 1, while in Fig. 15 iso-surfaces of hydrogen mass fraction (at 0.05) are plotted to analyse the mixture formation mechanism.

In Case "C", a clear separation of hydrogen and air is obtained during the injection, with almost no mixing. The H_2 jet directed towards the right bottom of the cylinder leads to a very rich pocket in the intake periphery that remains unmixed up to the end of the compression stroke. This is also related to the reduction of the tumble vortex intensity by the gas jet during the compression stroke (as visible in Fig. 16), that reduces the mixing effectiveness. Conversely, an improvement of the mixing is found injecting in favour of tumble (case "B"). The H_2 jet directed towards the left bottom of the cylinder creates a rich mixture pocket in that periphery that is spread out by the main tumble, the latter being further enhanced by the gas jet momentum in the same direction. As a result, charge homogeneity strongly worsens in case "C", while it improves in case "B", as shown in Fig. 17. The UI reduces by 15 % in case "C", while it increases by almost 5 % in case "B" with respect to the baseline case. Similarly, the *RMS* of λ reaches a value of 0.804 in case "C" and it is equal to 0.277 in case "B". Therefore, an improvement compared to the baseline case (characterized by an RMS value of 0.465) is obtained, as confirmed by the narrower *PDF*. Also the final turbulence level is affected by the hole orientation. An increase equal to 18 % of the average *TKE* at the compression stroke end is obtained when injecting in favour of the tumble vortex, visible from Fig. 16.

The performed sensitivity study highlights the primary role of the interaction between gas jet and organized cylinder motion. In the analysed high-tumble configuration, it is convenient to inject the hydrogen in favour of the main tumble vortex to emphasize its effect. In this way, the hydrogen is spread out by the bulk flow resulting in a more effective charge homogenization. On the contrary, injecting against tumble leads to accumulation of hydrogen in the intake periphery, resulting in a strongly asymmetric and inhomogeneous mixing at the compression stroke end.

4.2.3. Cases "D" to "H": 5- and 12-holes caps

A sensitivity to the hole number is performed moving to injector caps with 5 and 12 holes. The first 5-holes configuration (case "D") provides for one vertical plume and 4 jets whose radial orientation retains the combustion chamber geometrical symmetry. The hydrogen uniformly reaches the combustion chamber periphery, as visible in Fig. 18, where iso-surfaces of hydrogen mass fraction (at 0.05) are shown (while the mass fraction evolution on the symmetry plane is reported for the sake of completeness in Appendix 2). However, the resulting mixture homogeneity is worsened with respect to the baseline case, because of the interaction with the tumble motion. As shown in Fig. 19, a clear separation between the intake side (rich) and the exhaust one (lean) is obtained, similarly to case "C", with an *UI* of 77.6 % and a λ RMS of 0.671.

Following the previous outcomes obtained with the 3-holes caps, two exhaust-oriented 5-holes configurations are tested. The difference between cases "E" and "F" is the hole orientation with respect to the cylinder axis, which moves from 22° to 30°, respectively. In other words, case "F" is characterized by holes with less pronounced axial orientation.

The jet-wall interaction changes between "E" and "F" with the jets of the latter that directs the incoming fuel onto the cylinder liner rather than piston. The interaction with a fixed surface (liner, case "F") instead of a moving one (piston, case "E") obstacles the fuel-induced roll-up vortices formation (Fig. 18), despite this, the different holes orientation

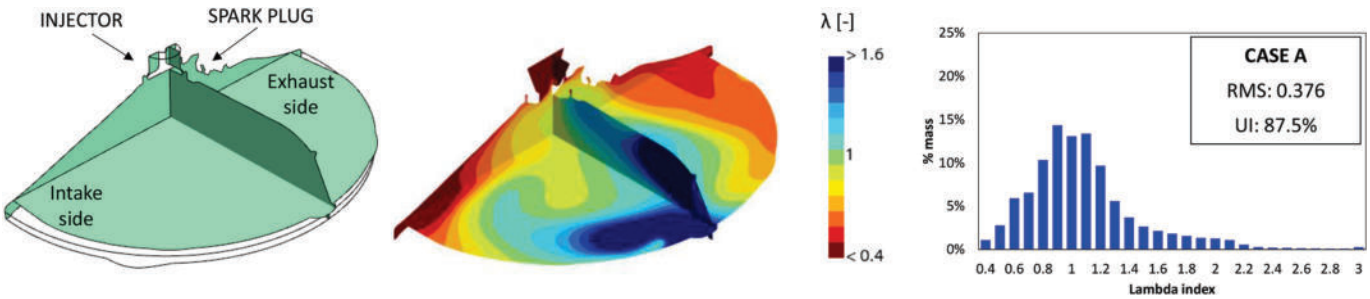

Fig. 13. Lambda distribution at 10 CAD bTDC obtained with the single-hole cap.

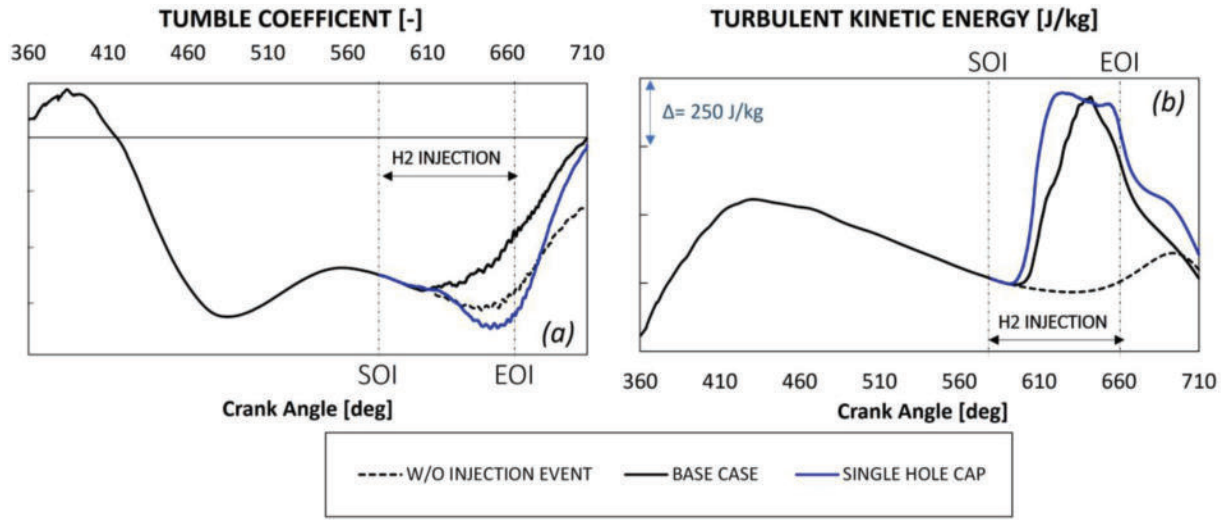

Fig. 14. Tumble intensity (a) and turbulent kinetic energy (b) obtained with the single hole cap.

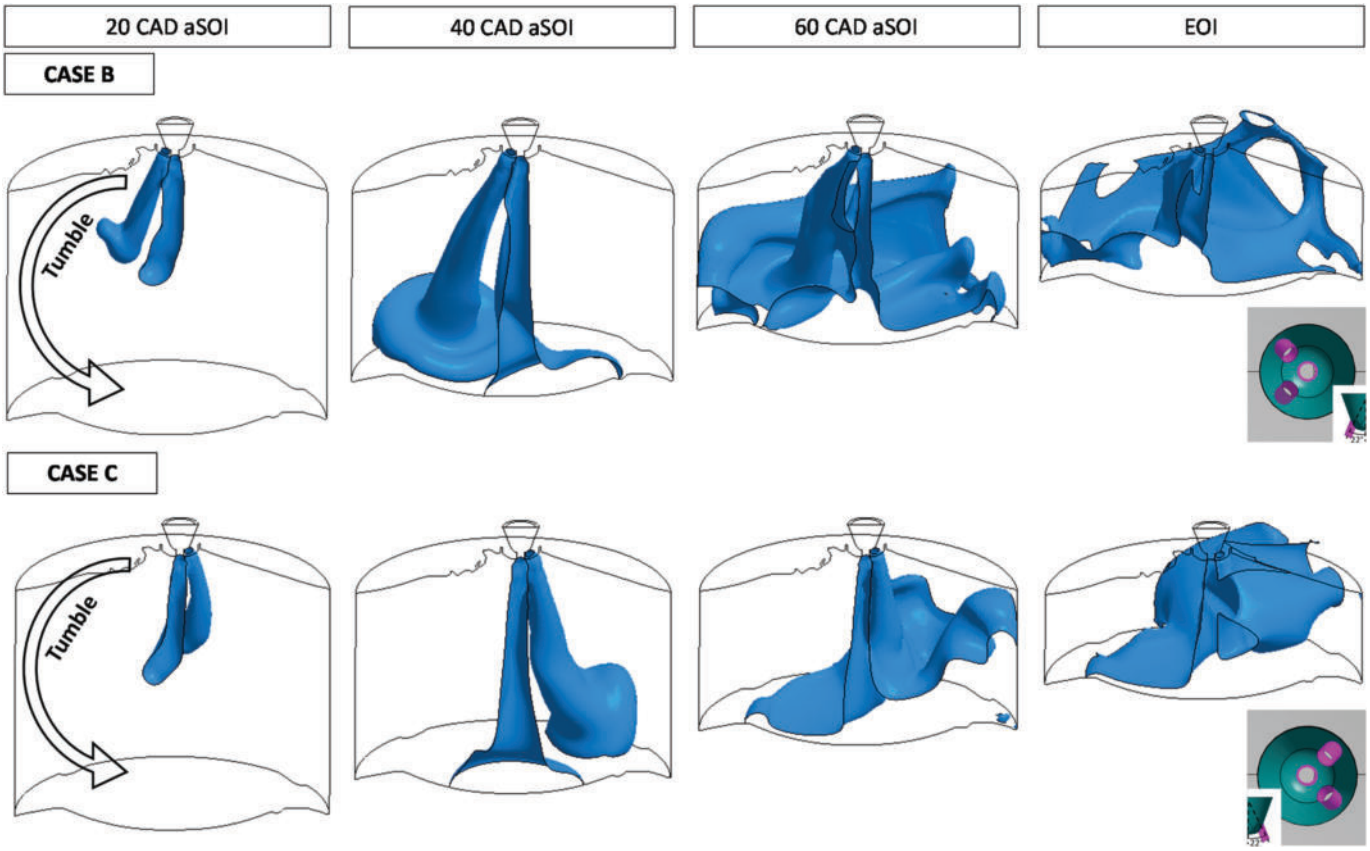

Fig. 15. Iso-surface of hydrogen mass fraction (at 0.05) for cases "B" and "C".

doesn't affect majorly the fuel distribution at the compression stroke end that presents the same macro-features. Fig. 19 shows a rich intake periphery and a lean exhaust one for both configurations, although the *UI* is 5 % higher in case "E" compared to case "F". This result highlights the relevant role of the jet-piston interaction on the final mixture homogeneity: the charge homogenization is enhanced by the jet interaction with the moving upwards piston crown rather than fixed liner.

In terms of turbulence and flow field, the exhaust-oriented configurations (cases "E" and "F") deliver the best results among the 5-hole injector caps, outperforming the uniform injection configuration (case "D"). This observation aligns with the trend previously identified in the 3-hole cap configurations (case "B," Fig. 16). Specifically, tumble-concordant injection proves more effective in enhancing the generation of the tumble vortex. As a result, it achieves the highest turbulence kinetic energy (*TKE*) at the end of the compression stroke (Fig. 20).

In order to spread out as much as possible the hydrogen inside the combustion chamber, two of fully symmetrical injection strategies based on 12-holes cap designs are tested. In the first one (case "G"), a uniform 30° radial spacing is considered, along with a hole tilt angle equal to 30° with respect to the cylinder vertical axis. In the second configuration

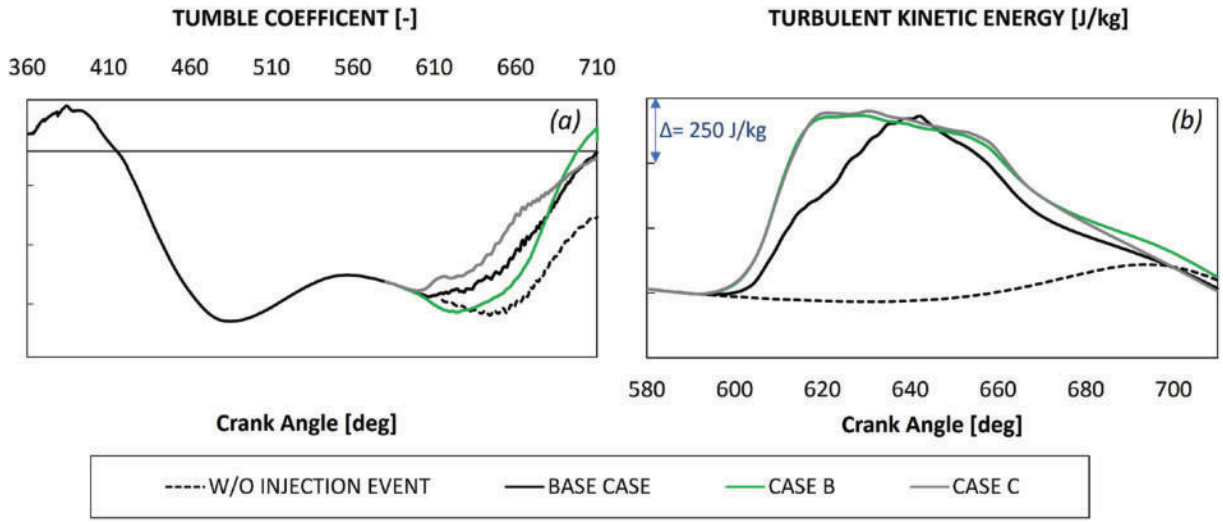

Fig. 16. Tumble (a) and turbulent kinetic energy (b) for cases "B" and "C".

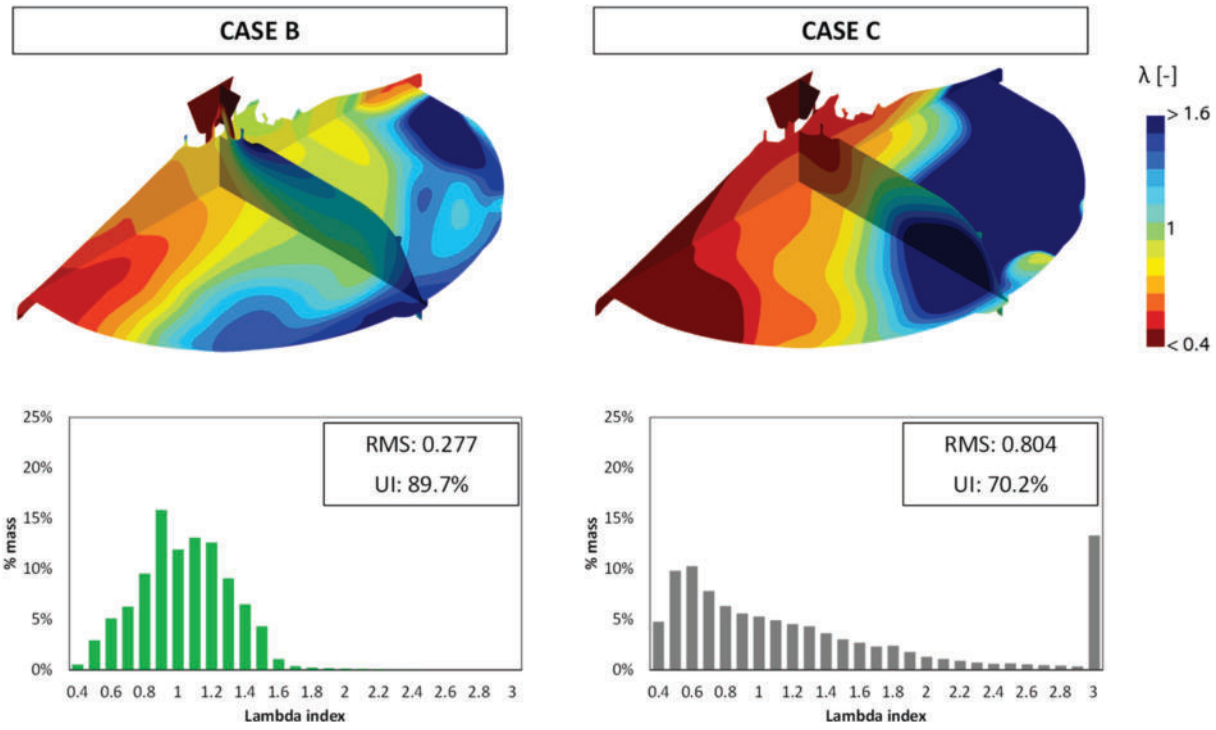

Fig. 17. Mixture stratification at 10 CAD bTDC for cases "B" and "C".

(case "H"), the holes are placed on two rows with a tilt angle of 30° for the upper row and of 15° for the lower one (Fig. 21).

As visible in Fig. 22 (and Appendix 2), the main difference between the two configurations is the jet collapsing. According to the literature, mixing improvement can be obtained by employing a high number of holes but, simultaneously, avoiding any jet collapse [21,59]. In case "G", partial merging of the jets occurs when injection starts, due to the low jet velocity. However, during the steady operation, the angular spacing is enough to avoid a full collapse of the plumes and to limit the penetration into the cylinder. The fuel remains bounded in the core of the combustion chamber with a less pronounced interaction with the walls, especially piston crown, during the compression stroke. The cap is effective in spreading out the fuel in the combustion chamber and the mixture homogeneity ($UI = 87.4$ %) is improved compared to the baseline case. In the dual-row configuration (case "H"), the wider angular spacing should avoid the jet collapse, thus improving the mixture homogeneity. However, the 15° tilt angle of the holes of the lower row enhances the plume interaction with the piston crown: the mixture evolution is similar to the baseline case and the final result is a worsening of the charge homogeneity ($UI = 81.7$ %). Fig. 23 compares the fuel stratification at the compression stroke end. Rich and lean mixture pockets like the baseline case are detected in case "H", while an improvement of the mixture homogeneity in case "G" is evident. This last configuration is the only one able to eliminate the lean mixture pocket in the exhaust periphery, while almost no fuel reaches the intake one. Turbulence and Tumble are very similar comparing case "H" to the baseline one, while tumble vortex intensity is slightly enhanced in case "G", where no jet collapse occurs, as visible in Fig. 24.

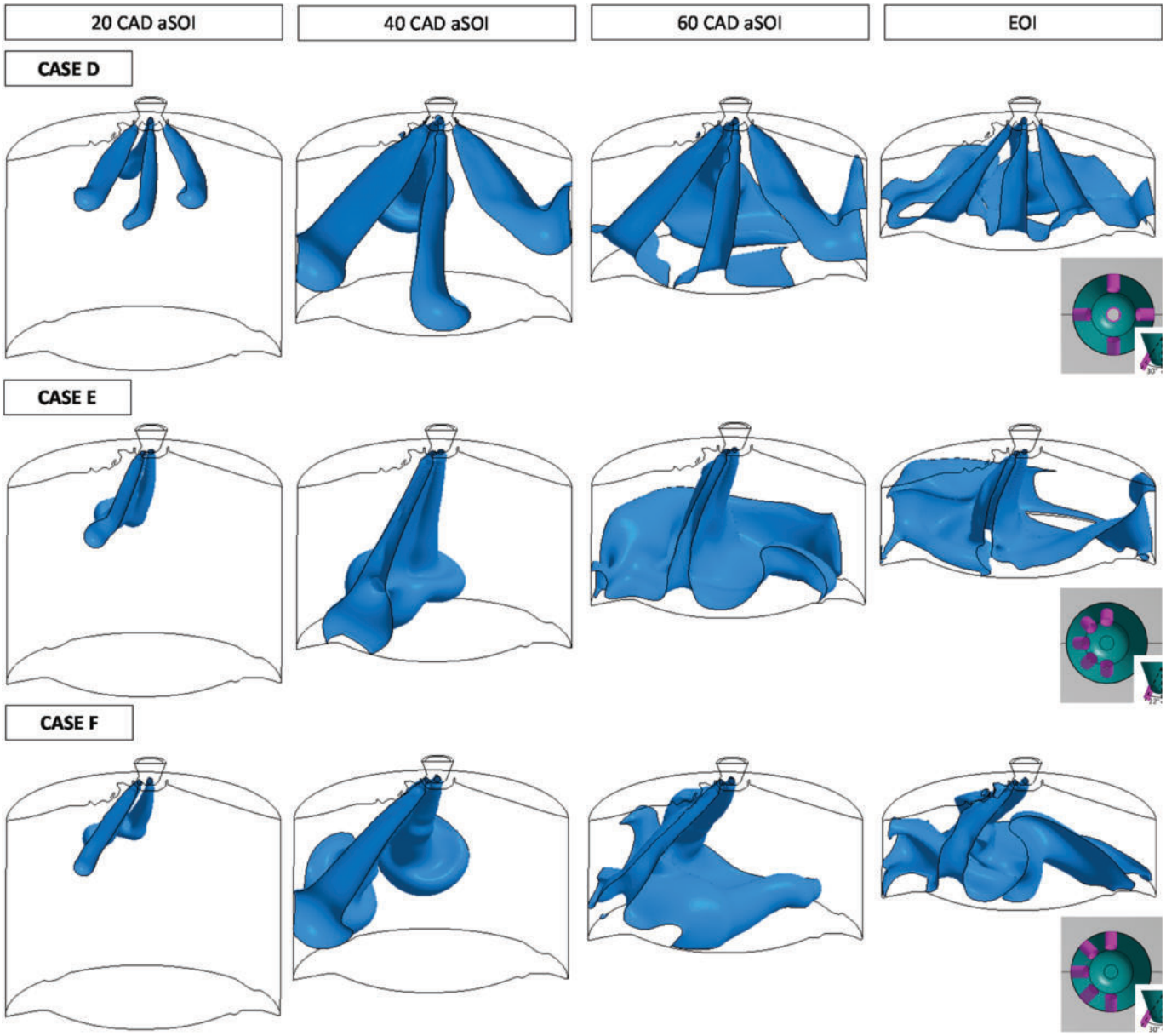

Fig. 18. Iso-surface of hydrogen mass fraction (at 0.05) for cases "d", "e" and "f".

4.2.4. Mixture formation: a wrap up

Different injector cap geometries are realized and tested with the final aim to improve the mixture homogeneity at compression stroke end, when adopting a late injection strategy in a high-tumble engine configuration. Opposite strategies are adopted. Some of them try to concentrate and orient the hydrogen jets towards preferential directions in the combustion chamber by employing a low number of holes. Others spread as much as possible the fuel via symmetric configurations and higher holes number.

- Regarding the first strategy, an improvement of the mixture formation is found when the jet-piston interaction is enhanced with a single vertical hole configuration or when injecting (with both 3 and 5 holes) in favour of the main tumble vortex, that helps to spread out the hydrogen in the combustion chamber. A strong worsening of the mixture preparation is obtained when injecting against the incoming air flux. Regarding the tilt angle, better results are obtained with low values, i.e. it is preferable to orient the jets towards the piston crown rather than to the cylinder liner.
- Configurations with a high hole number can also be effective in improving the mixture, provided that no jet collapse is obtained and jet-wall interactions are reduced. The 12-holes configuration with a 30° tilt angle is proved to be effective to spread out the hydrogen in the combustion chamber.

The Uniformity Index (*UI*) and the λ RMS values for all the simulated cases are summarized in Table 3, together with turbulence related quantities. With respect to the baseline configuration without injector cap, four designs improve the charge homogeneity: the single hole cap ("A"), the 3- and 5-holes designs with exhaust-oriented drilling ("B" and "E") and the 12-holes single-row configuration ("G"). Conversely, the other tested geometries worsen the mixture homogeneity compared to the baseline configuration.

The single hole cap is the best in terms of *TR* peak and *TKE* improvement at the compression stroke end. In addition, it ensures an enrichment of the spark plug region. Case "B" presents the optimal homogeneity, which is achieved with an enhanced tumble ratio. Case "E" maintains the same injection direction of "B" but with a higher number

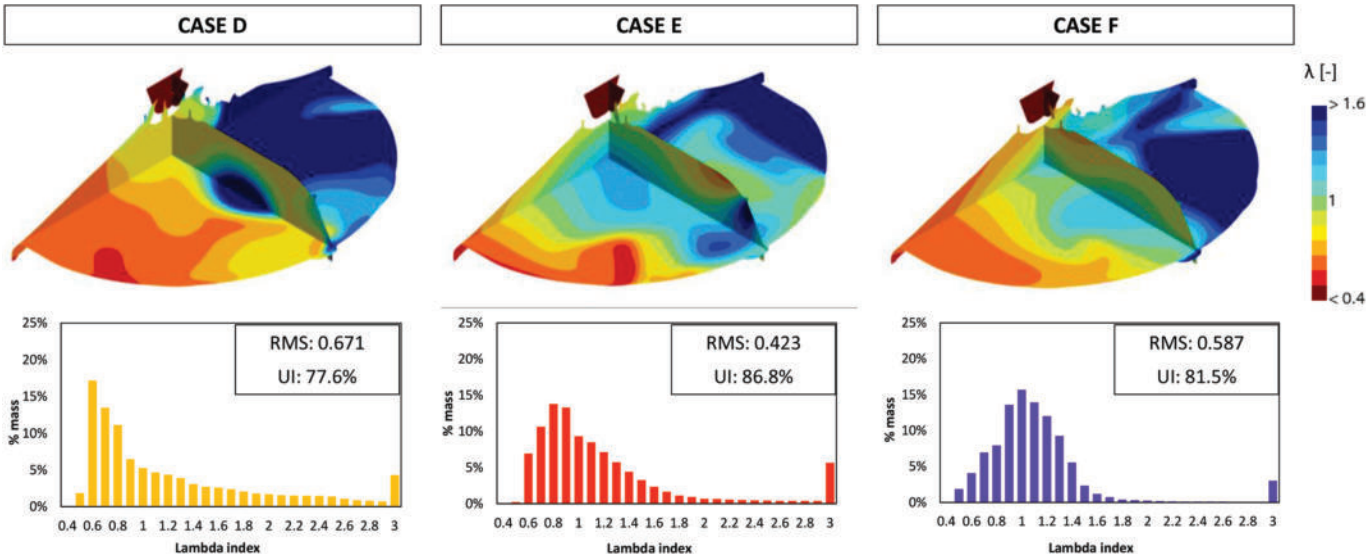

Fig. 19. Lambda distribution at 10 CA bTDC for the 5-holes cap configurations.

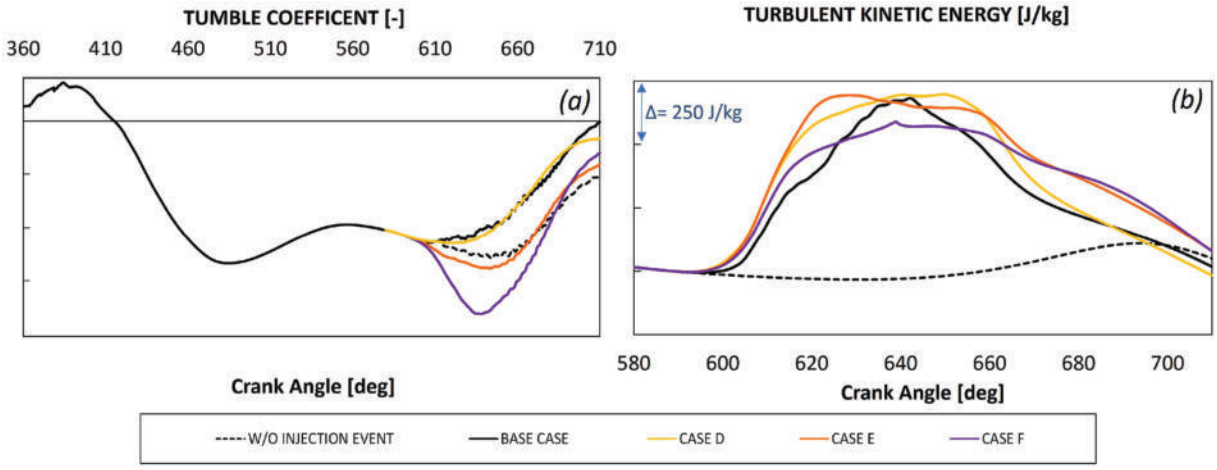

Fig. 20. Tumble (a) and turbulent kinetic energy (b) behaviour with the different 5-holes cap designs.

of holes and it exhibits a lower uniformity improvement but higher tumble and turbulence enhancement at the end of the compression. The case "G" (12-holes) slightly improves the mean turbulence without enriching the mixture close to the spark-plug.

Considering, for the different configurations ("A", "B", "E" and "G"), the very similar *UI* and the quite different values of both λ in the spark region and average turbulence at the compression stroke end, it is difficult to rank the most promising cap design. For this reason, combustion is simulated in the four best cases, to numerically assess and quantify the impact of the different charge stratifications and turbulence levels. The combustion results are reported and analysed in the following section.

4.3. Combustion analysis

Combustion is simulated using the setup defined for the baseline case validation. Performance indicators and flame front evolution are adopted to compare the different injector cap designs. As a first step, all the cases are simulated adopting the same spark time of the baseline configuration (6 *CAD bTDC*) and the main results are summarized in Fig. 25. The higher mixture homogeneity of the selected cases is effective in improving the combustion duration, that reduces for all the tested configurations. The early combustion duration is positively affected by the change of mixture quality in the spark region, which improves in all the cases. This is coherent with the existing literature that confirms the importance of a slightly rich mixture close to the spark plug to improve combustion duration and stability [36]. In this regard, cases "A" and "B" are the ones showing the most significant ignition delay (*MFB* 0–10 %) reduction and, consequently, the most advanced combustion phasing. In particular, case "A" is characterized by a 20 % higher pressure peak compared to the baseline case, resulting in a 6 % increase of the *IMEP* value. Despite the enrichment at the spark-plug and the resulting advanced combustion phasing, case "B" shows only a 5 % reduction of the combustion duration, due to the leaner periphery. As shown in Fig. 23, case "G" is the one presenting the greater portion of the cylinder at stoichiometric conditions. The absence of optimal mixture close to the spark-plug leads to a slight delay in the combustion phasing, but the higher overall homogeneity reflects in a 21 % reduction of the combustion duration. The best result in terms of combustion duration is observed in case "E", where the enhancement of the tumble intensity achieved by orienting the hydrogen jets promotes a more rapid flame propagation. However, the presence of extra-lean zones as in the combustion chamber periphery of cases "B" and "E" leads to higher concentration of unburned H_2 and lower combustion efficiency, as visible in

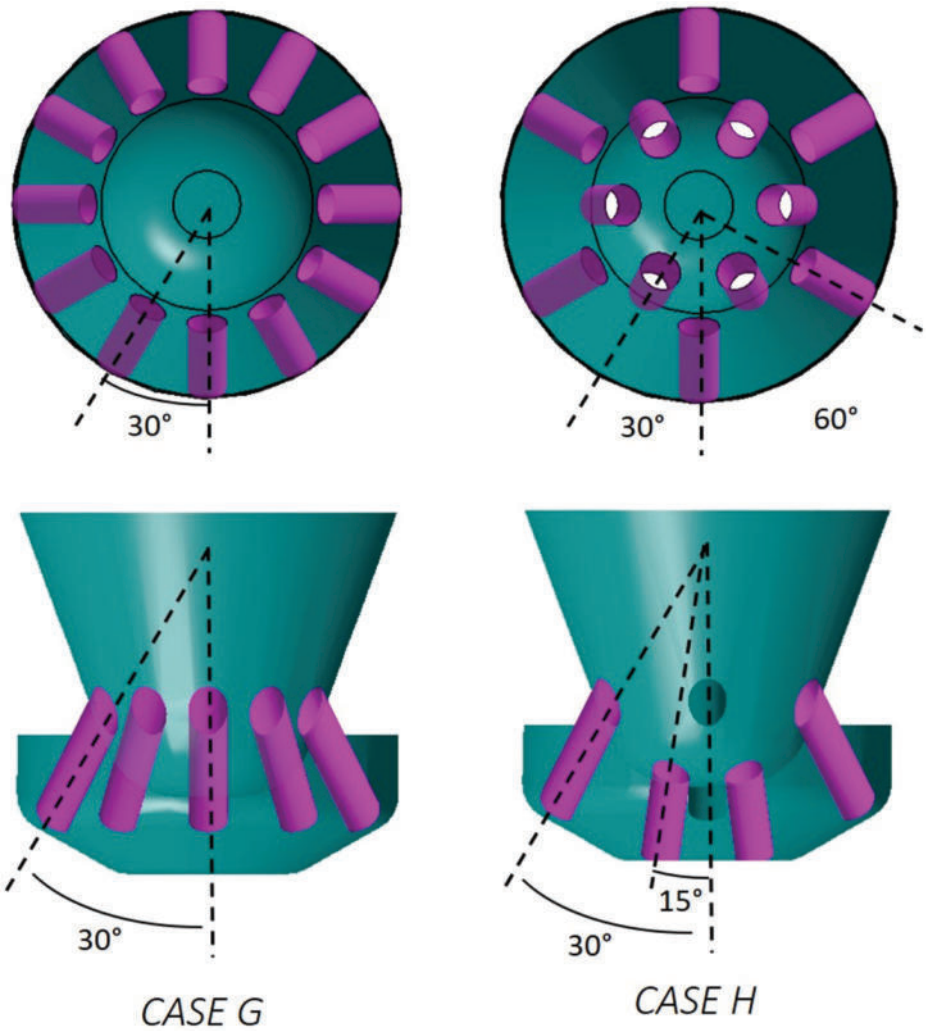

Fig. 21. 12 holes cap design details.

Table 4.

For a fairer comparison of the combustion evolution between the selected cases, i.e. to avoid duration improvements related to advanced combustion phasing rather than to mixture quality, the cases are repeated varying the spark advance and targeting the same combustion phasing (*MFB* 50 %) of the baseline configuration (12.8 *CAD*). Due to the mixture quality improvements, the spark time is delayed for all the cases, with the biggest variation (~4 *CAD*) applied to case "A" and the smallest one (~0.5 *CAD*) to case "G". The comparison between the cases in terms of pressure, heat release rate and mass fraction burnt is reported in Fig. 26. As visible in Table 4, on equal combustion phasing, pressure peak and *IMEPH* are now more similar among the cases, and the differences between the latter and the baseline case are reduced if compared to the previous analysis. The maximum increase in the pressure peak (~8 %) and *IMEPH* (~4 %) is found for case "E", the one showing the higher advantage in terms of combustion duration (−29.6 %). The general improvement of the mixture homogeneity in the combustion chamber directly affects the first half of the combustion duration, that decreases for all the cases with a maximum reduction of 24 % in case "E" and a minimum one of 13 % in cases "A" and "B". Higher differences are found when the flame approaches the combustion chamber periphery. Only case "E" and "G" are able to reduce the *MFB* 50–90 %, while an increase is found in cases "B" and "E", which are the ones showing the periphery with the widest lean portion. As for case "A", the duration is like the baseline one. The presence of wide lean mixture pockets is also responsible for the combustion efficiency reduction. The improved charge homogeneity of case "G" that leads to nearly stoichiometric mixture also in the combustion chamber periphery (except for a small lean pocket on the intake side) helps the flame propagation after the *MFB* 50 %. This results in a faster combustion with respect to the baseline configuration (the *MFB* 10–90 % reduces of 17.3 %). Thanks to the improvement of the *MFB* 10–50 %, the overall combustion duration slightly shortens in cases "A" and "E" (of 4 % and 3.4 %, respectively). Because of the delay in the *MFB* 50–90 %, the *MFB* 10–90 % minimally increases in case "B" (of 2 %). In spite of worse mixing in the exhaust periphery, thanks to the highest turbulence level, Case "E" is the one well performing in terms of second half and global combustion duration highlighting the first order role of turbulence in improving combustion when the flame approaches the cylinder walls.

Despite The good correlation between mixture quality and combustion results, the strong improvement of the *MFB* 50–90 % in the 5-holes configuration is mainly related to higher turbulence while, in the 12-holes configuration cannot be fully ascribed to turbulence increase and different charge stratification.

Analysing the flame front evolution in the baseline case, a strong asymmetry in the flame propagation direction is visible. Because of the spark plug position, the flame reaches the exhaust periphery much earlier than the intake one. This occurs although the mixture quality (richer in the intake periphery) suggests an opposite behaviour. Comparing the baseline case with the best performing one (namely "G"), a strong reduction in the flame propagation asymmetry can be noticed, despite the leaner intake periphery. This confirms that fuel stratification

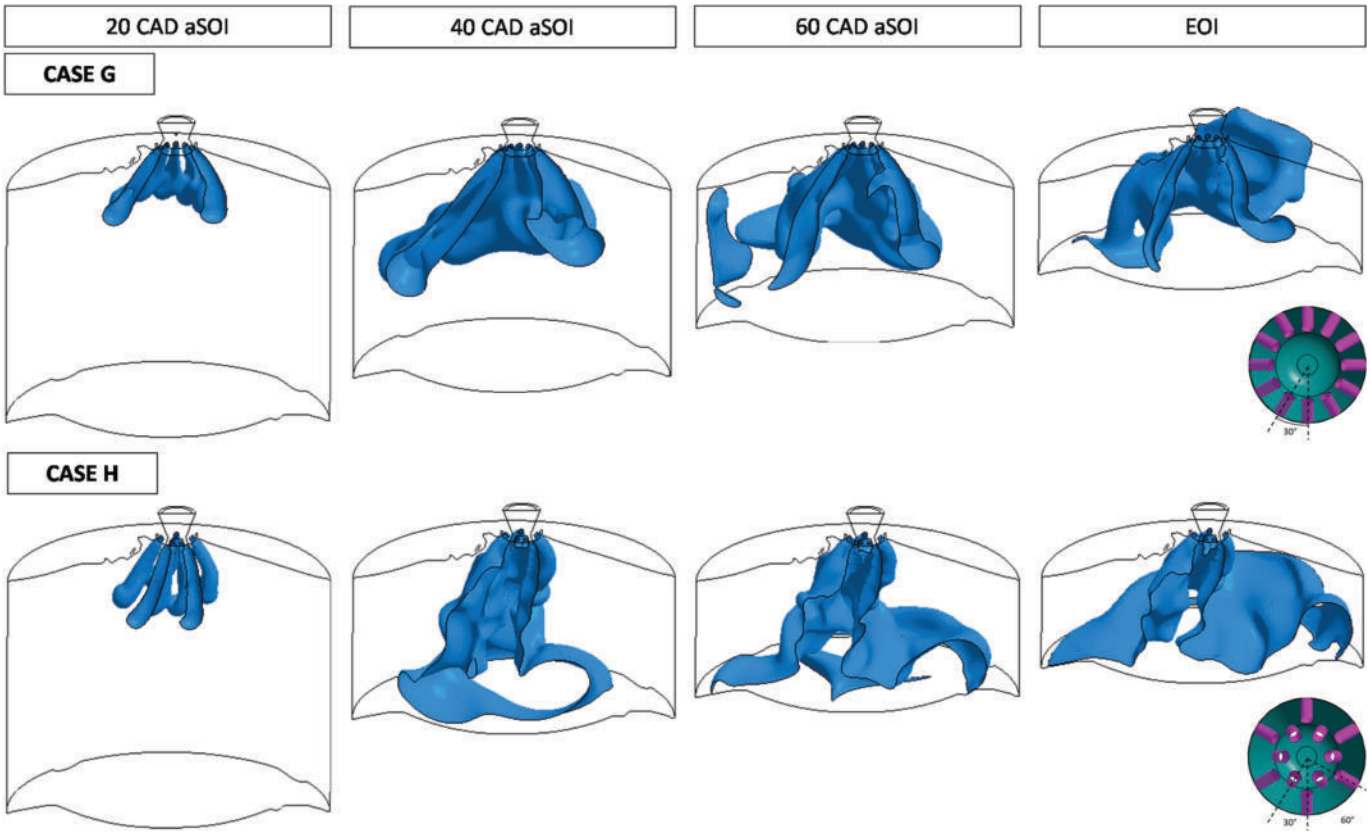

Fig. 22. Iso-surface of hydrogen mass fraction (at 0.05) for cases "G" and "H".

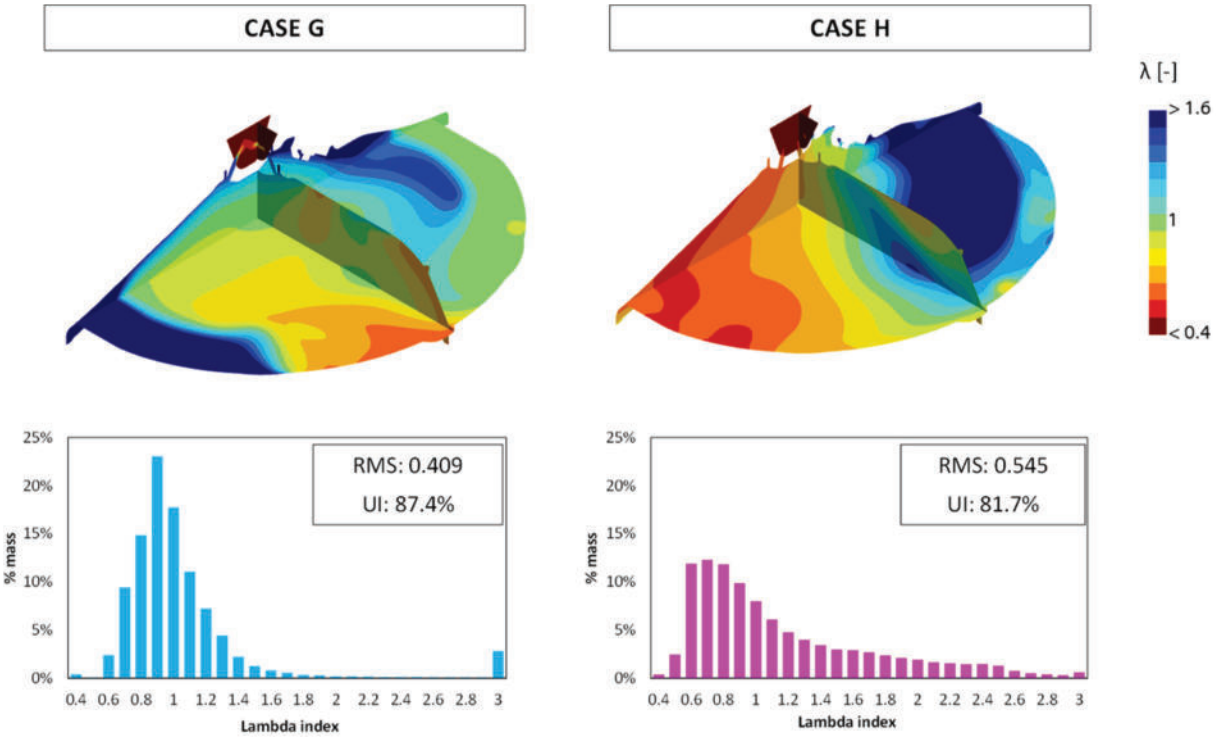

Fig. 23. λ distribution at 10 CA bTDC for the 12-holes cap configurations.

is not the only aspect to consider optimizing combustion. For the sake of completeness, images of the flame on two different section planes are reported in Appendix 3 for both baseline and "G" cases.

The asymmetrical flame propagation of the baseline case is related to the flow field in the combustion chamber, specifically to the main tumble vortex evolution. As previously discussed, the hydrogen

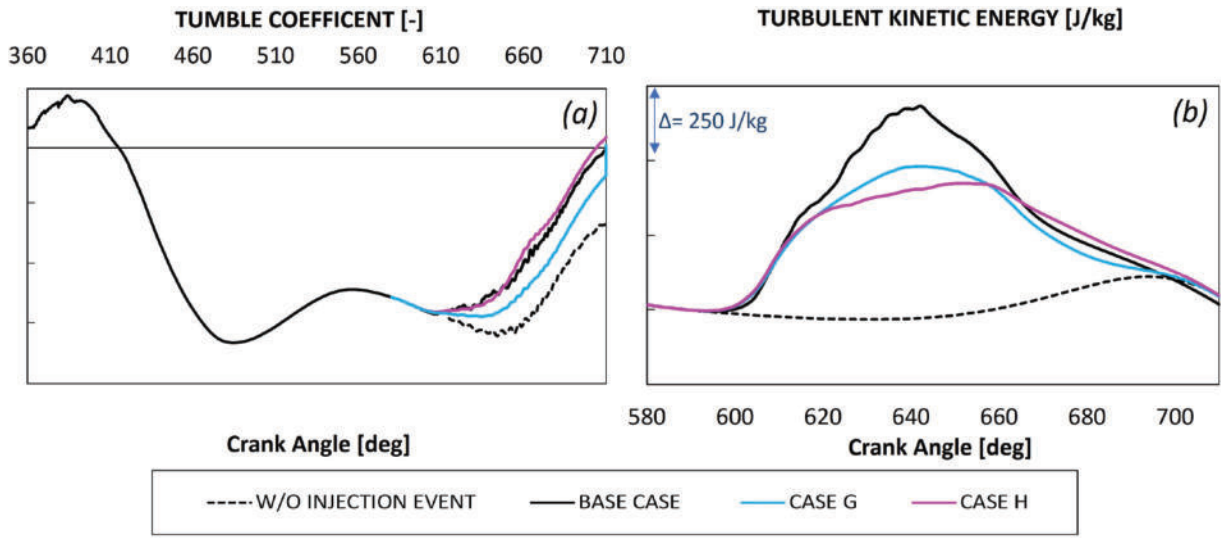

Fig. 24. Tumble (a) and turbulent kinetic energy (b) behaviour with the different 12-holes cap designs.

Table 3
Performance parameters of the tested caps.

Case Name	Description	UI	Lambda RMS	Lambda @Spark	TKE @Spark	Peak of Tumble Ratio	Δ(U.I.)%
Baseline	Pintle injector configuration	85.1 %	0.465	1.26	-	-	-
*A**	Single axial hole	87.5 %	0.376	0.84	33 %	31 %	2.4 %
*B**	3-Holes exhaust oriented (22°)	89.7 %	0.277	0.89	17 %	16 %	4.6 %
C	3-Holes intake oriented (22°)	70.2 %	0.804	0.57	−4 %	−8 %	−14.9 %
D	5-Holes symmetric (30°)	77.6 %	0.671	0.97	−13 %	4 %	−7.5 %
*E**	5-Holes exhaust oriented (22°)	86.8 %	0.423	1.02	24 %	28 %	1.7 %
F	5-Holes exhaust oriented (30°)	81.5 %	0.587	1.16	23 %	67 %	−3.6 %
*G**	12-Holes single-row (30°)	87.4 %	0.409	1.3	10 %	5 %	2.3 %
H	12-Holes dual-row (30°/15°)	81.7 %	0.545	0.95	11 %	−1 %	−3.4 %

injection in the baseline case leads to faster dissipation of the tumble with a TR that is almost zero at the spark time (Fig. 10). The resulting flow field at the combustion start is reported in Fig. 25. The almost zero residual tumble leads to a strong exhaust-oriented and non-rotating flow field, which is responsible for the asymmetric flame propagation and able to overcome the effect of the charge stratification. This is confirmed by the laminar flame speed field reported in Fig. 27, which would suggest a faster propagation of the flame on the intake side. Conversely, with the 12-holes injector cap, the interaction between gas jets and tumble vortex is lower. Therefore, the tumble dissipation is less affected by the gas injection, showing a behaviour more similar to the reference case without injection. Thanks to this, the residual tumble motion at the spark time is not negligible and a rotating flow structure is maintained, which is responsible for a faster flame propagation towards the intake side. The different injection-flow interaction is also responsible for the increase of the final turbulence intensity in case "G" that further enhances the flame propagation and it is responsible for the combustion duration improvement. In this regard, also the turbulent kinetic energy is reported in Fig. 27.

This last analysis confirms the complex interactions between mixture quality, turbulence, flow field and combustion evolution as well as the importance of simulating combustion to define the best strategy for the hydrogen injection, when the final goal is the optimization of the combustion process itself.

5. Conclusions

The optimization of the mixture formation represents a major challenge for the development of H_2-DI engines. Indeed, charge stratification significantly impacts on combustion evolution, knock and pre-ignition occurrence and emission formation. In this scenario, injector caps can be proficiently adopted to affect the mixture formation by varying the incoming gas jet orientation in the combustion chamber, without the need for a complete re-design of the hydrogen injector. The main issue related to the development of an injector cap for a specific engine application is related to the countless possible designs to be explored. For this reason, the definition of design guidelines is crucial to reduce efforts and time needed for the engine optimization.

3D-CFD simulations of the hydrogen-air mixing in the combustion chamber can be effective to identify design guidelines for a specific engine application. In fact, they offer the possibility to deepen the complex interaction between gas-jet, organized flow, cylinder walls and turbulence faster and more efficiently than with complex and costly experimental tests. However, numerical models must be validated before their adoption to explore designs.

In the current work, the potentials of injector caps to improve mixing and combustion performance of a high-performance *H_2-DI* engine are investigated by 3D-CFD simulations. The reliability of the numerical model is verified by comparing CFD results with available experimental data on both gas jet evolution and combustion. A reasonable compromise between simulation accuracy and computational effort is found. The baseline engine case (without injector cap) is simulated and adopted as a benchmark for the new configurations aiming at improving the mixture homogeneity, at the end of the compression stroke, when adopting a delayed injection strategy. Different injector caps are designed, with variable hole orientation, number and diameter. They are numerically tested on equal mass flow rate and injection phasing.

From the performed CFD analysis, conclusions of general validity can be derived.

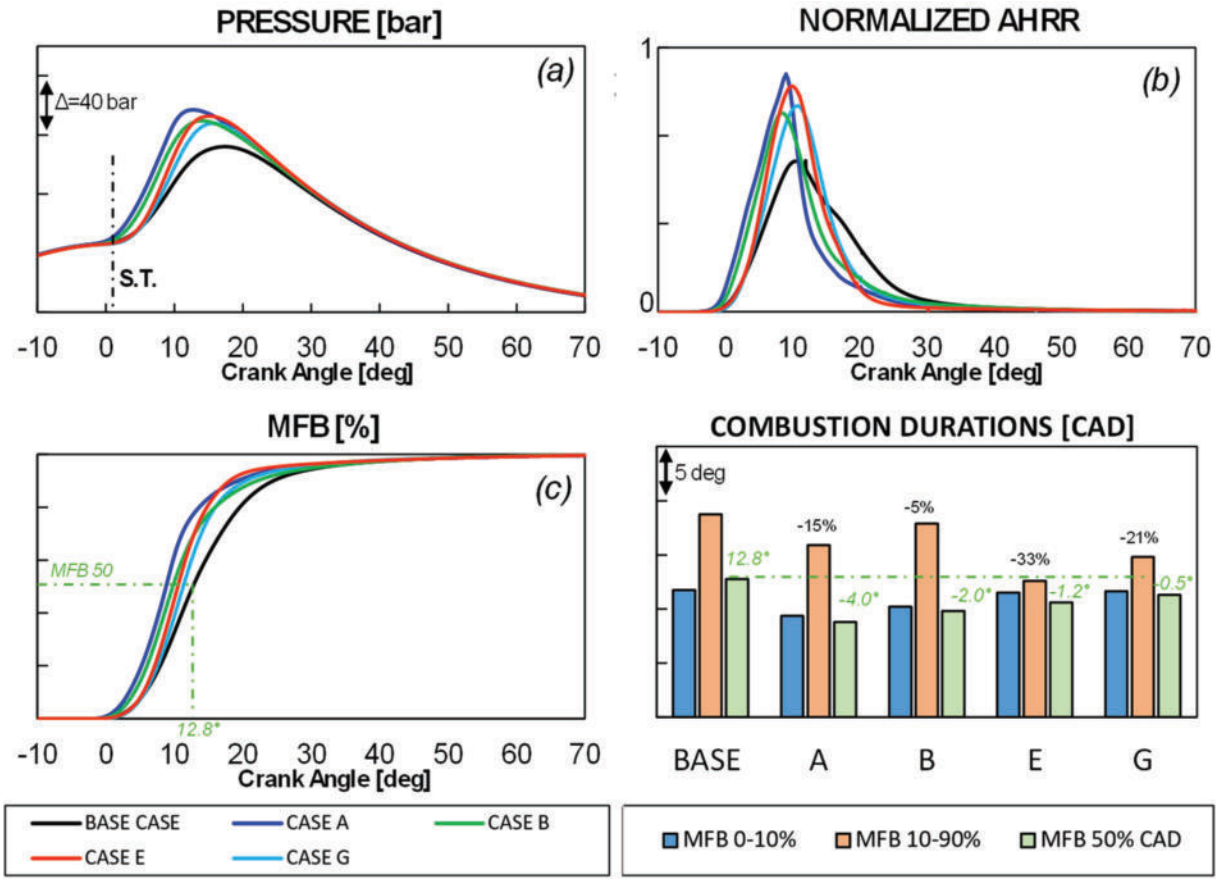

Fig. 25. Cylinder pressure (a), apparent heat release rate (b), MFB (c) and combustion indicators (d), on equal spark time, for the most promising cap designs.

Table 4
Main combustion results for the two analysed conditions, namely equal combustion start and equal combustion phasing.

	CASE A	CASE B	CASE E	CASE G
COMBUSTION RESULTS WITH RESPECT TO BASE CASE AT FIXED SPARK TIME = -6 CA				
Δ(PEAK pressure)%	18.8 %	13.2 %	15.6 %	12.0 %
Δ(IMEPH)%	5.8 %	5.5 %	5.7 %	5.2 %
Δ(MFB 10–90)%	−15.2 %	−4.5 %	−32.8 %	−21.1 %
COMB. EFFICIENCY (BASE = 99.22 %)	99.36 %	98.87 %	98.91 %	99.40 %
COMBUSTION RESULTS WITH RESPECT TO BASELINE CASE AT SAME MFB50 %				
Δ(PEAK pressure)%	6.6 %	3.6 %	8.3 %	7.4 %
Δ(IMEPH)%	2.8 %	3.0 %	3.9 %	4.0 %
Δ(MFB 0–10)%	−15.0 %	−11.0%	+1.0 %	0.0 %
Δ(MFB 10–50)%	−13.0 %	−14.0 %	−24.2 %	−16.0 %
Δ(MFB 50–90)%	+1.0 %	+12.0 %	−32.8 %	−18.0 %
Δ(MFB 10–90)%	−4.0 %	2.4 %	−29.6 %	−17.3 %
COMB. EFFICIENCY (BASE = 99.22 %)	99.43 %	98.70 %	98.74 %	99.36 %

- Hydrogen injection significantly impacts on the evolution of tumble motion and turbulence in the combustion chamber. Depending on the injector configuration, tumble can be promoted or suppressed, leading to non-negligible variations in both flow field and turbulence intensity at the compression stroke end. Such variations influence, in turn, the flame propagation.
- Injecting in favour of tumble improves the hydrogen spread in the combustion chamber, enhancing mixture homogeneity and cylinder turbulence.
- The interaction between hydrogen jets and combustion chamber walls has a primary role on the mixture homogenization too. In particular, the interaction between a straight and narrow axial jet (obtained with a single hole cap) with the piston crown is effective to improve both mixing and turbulence with respect to a more spread hydrogen jet resulting from injection without cap.
- Symmetric cap configurations are effective to improve mixture homogeneity if the number of holes is kept as high as possible and, simultaneously, jet collapse is avoided.
- In general, combustion performance is improved by the increase of mixture homogeneity. Nevertheless, mixing is not the only parameter to consider. Other aspects such as residual tumble motion and turbulence can significantly impact on the flame propagation, especially after the *MFB* 50 %. The complex interaction between the above factors can be effectively studied by CFD simulations including necessarily combustion analyses.
- Charge stratification plays a primary role in the first half of the combustion process, including ignition delay, while the second half is predominantly influenced by turbulence and flame propagation direction due to in-cylinder flow field.
- Focusing on cold flow and mixing the best charge homogeneity is obtained with a 3-hole configuration injecting in favour of the main tumble (Case “B”)
- Among the tested configurations, Case “E” demonstrated the best engine performance and combustion duration. While it is not the most effective in terms of mixing improvement, it achieves one of the highest turbulence levels at the start of combustion, contributing to its superior performance.

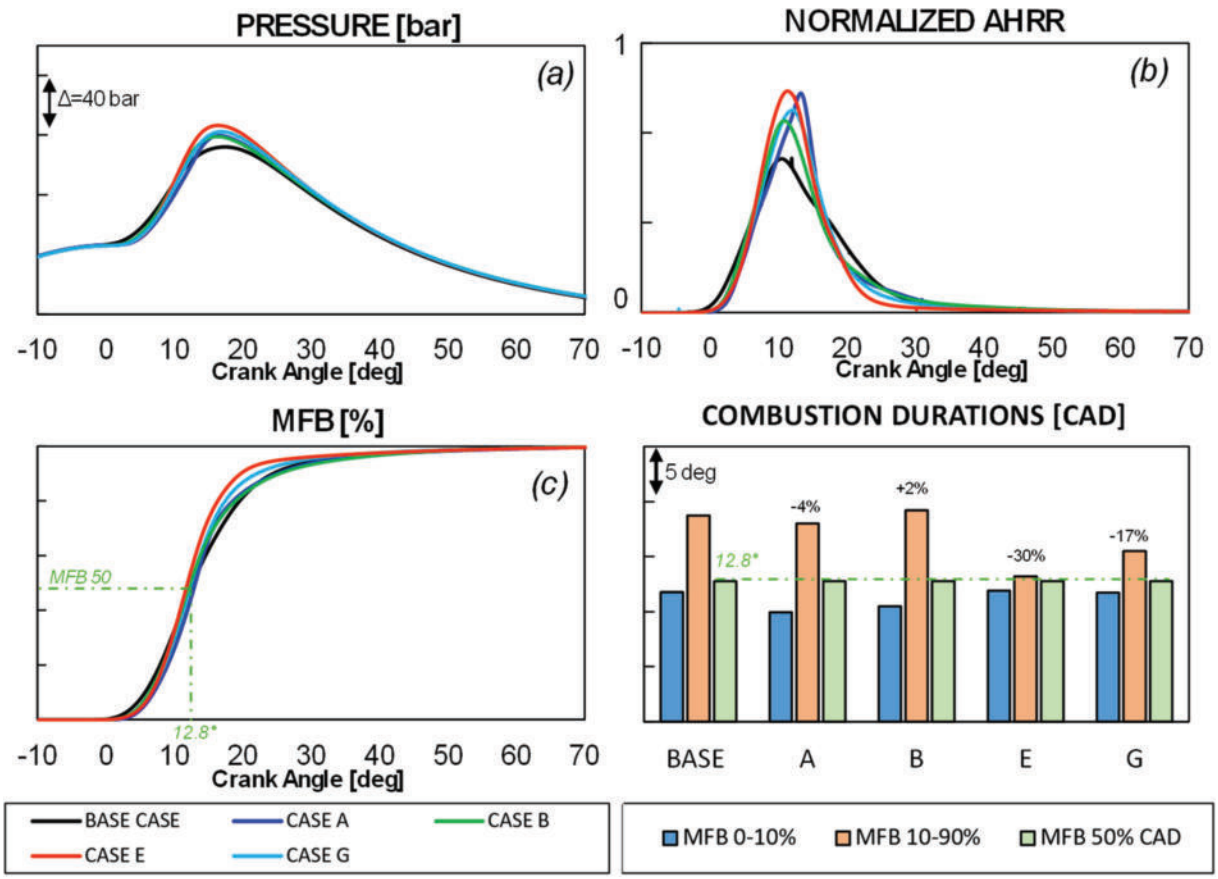

Fig. 26. Cylinder pressure (a), apparent heat release rate (b),MFB (c) and combustion indicators (d), on equal combustion phasing (MFB-50 %), for the most promising cap designs.

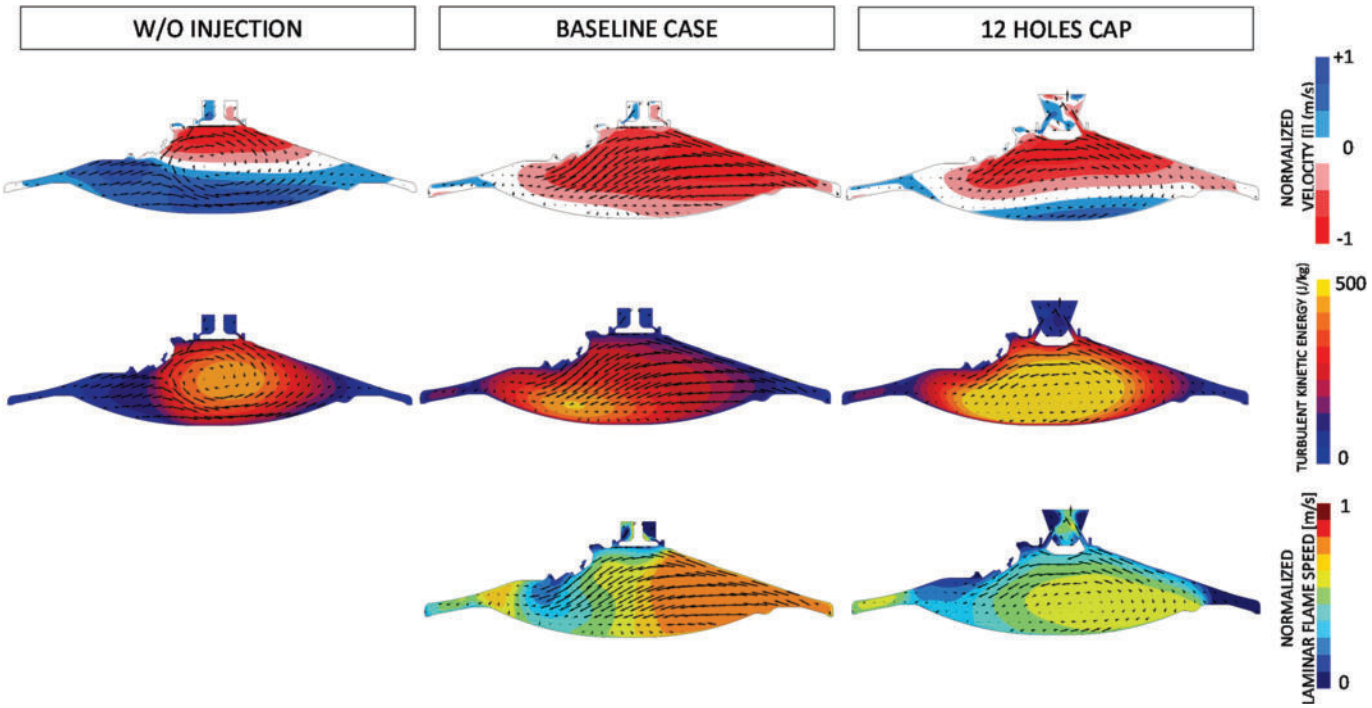

Fig. 27. Comparison between baseline case and 12-holes cap ("g") in terms of velocity field, at 10 CAD bTDC.

The mixture formation in a high-performance hydrogen engine is crucial not only to improve the combustion performance, but also to avoid pre-ignition and knock as well as to reduce NO_x emissions. The proposed numerical framework will be further extended and validated to account for these important aspects, with the aim to develop design guidelines to reduce abnormal combustion occurrence and NO_x emissions.

CRediT authorship contribution statement

Sebastiano Breda: Writing – review & editing, Writing – original draft, Visualization, Validation, Supervision, Methodology, Formal analysis, Data curation. **Veronica Patrizi:** Writing – original draft, Visualization, Validation, Software, Methodology, Investigation, Formal analysis, Data curation, Conceptualization. **Fabio Berni:** Writing – review & editing, Writing – original draft, Validation, Supervision, Investigation, Formal analysis, Conceptualization. **Roberto Tonelli:** Writing – review & editing, Validation, Supervision, Methodology, Investigation, Formal analysis. **Fabio Santi Mortellaro:** Writing – review & editing, Validation, Supervision, Methodology, Formal analysis. **Stefano Fontanesi:** Writing – review & editing, Supervision, Resources, Project administration, Methodology, Funding acquisition, Formal analysis, Conceptualization.

Declaration of competing interest

The authors declare the following financial interests/personal relationships which may be considered as potential competing interests:

Sebastiano Breda, Stefano Fontanesi and Veronica Patrizi report financial support was provided by European Union, NextGenerationEU - National Sustainable Mobility Center - MOST, CN00000023, Italian Ministry of University and Research, Spoke 12 (CUP E93C22001070001). If there are other authors, they declare that they have no known competing financial interests or personal relationships that could have appeared to influence the work reported in this paper.

Acknowledgments

The authors acknowledge the support provided by “European Union-Next generation EU trough the “PIANO NAZIONALE DI RIPRESA E RESILIENZA (PNRR) – MISSION 4 COMPONENTE 2, “Dalla ricerca all’impresa” INVESTIMENTO 1.4, (CN00000023). In the context of the “Sustainable Mobility Center (Centro Nazionale per la Mobilità Sostenibile – CNMS)” - Spoke 12 - Avviso MUR 3138/2021 modificato con DD 3175/2021”

Appendix A. Supplementary data

Supplementary data to this article can be found online at https://doi.org/10.1016/j.ijhydene.2025.05.085.

List of Abbreviations

BMEP	Brake Mean Effective Pressure
bTDC	before Top Dead Centre
CAD	Crank Angle Degree
CFD	Computational Fluid Dynamics
CO2	Carbon Dioxide
DI	Direct Injection
EOI	End of Injection
ECFM	Extended Coherent Flamelet Model
EU	European Union
FCEV	Fuel Cell Electric Vehicle
GDI	Gasoline Direct Injection
GHG	Greenhouse Gas
H2	Hydrogen
ICE	Internal Combustion Engine
IVC	Intake Valve Closing
IEA	International Energy Agency
IMEP	Indicated Mean Effective Pressure
Lambda	Air-Fuel equivalence ratio
LFS	Laminar Flame Speed
MFB10-90	10-90 %of Mass Fuel Burned
MFB50	50 % of Mass Fuel Burned
NOx	Nitrogen Oxide
PFI	Port Fuel Injection
PISO	Pressure-Implicit With Splitting of Operations
RANS	Reynolds Averaged Navier Stokes
SOI	Start od Injection
SCE	Single Cylinder Engine
SI	Spark Ignition
TDC	Top Dead Centre
TKE	Turbulent Kinetic Energy
TFS	Turbulent Flame Speed

References

[1] The European Green Deal.” Available Online at: https://commission.europa.eu/strategy-and-policy/priorities-2019-2024/european-green-deal_en.
[2] Greenhouse gas emissions from transport in Europe.” Available Online at: https://www.eea.europa.eu/en/analysis/indicators/greenhouse-gas-emissions-from-transport?activeAccordion.
[3] Yip HL, Srna A, Yuen ACY, Kook S, et al. A review of hydrogen direct injection for internal combustion engines: towards carbon-free combustion. Appl Sci 2019;9(22):4842. https://doi.org/10.3390/app9224842.
[4] Stępień Z. A comprehensive overview of hydrogen-fueled internal combustion engines: achievements and future challenges. Energies 2021;14(20):6504. https://doi.org/10.3390/en14206504.
[5] Sun Z, Hong J, Zhang T, Sun B, et al. Hydrogen engine operation strategies: recent progress, industrialization challenges, and perspectives. Int J Hydrogen Energy 2023;48:366–92. https://doi.org/10.1016/j.ijhydene.2022.09.256.
[6] Verhelst S, Sierens R. Hydrogen engine-specific properties. Int J Hydrogen Energy 2001;26:987–90. https://doi.org/10.1016/S0360-3199(01)00026-X.
[7] White CM, Steeper RR, Lutz AE. The hydrogen-fueled internal combustion engine: a technical review. Int J Hydrogen Energy 2006;31:1292–305. https://doi.org/10.1016/j.ijhydene.2005.12.001.
[8] Navale SJ, Kulkarni RR, Thipse SS. An experimental study on performance, emission and combustion parameters of hydrogen fueled spark ignition engine with the timed manifold injection system. Int J Hydrogen Energy 2017;42:8299–309. https://doi.org/10.1016/j.ijhydene.2017.01.059.
[9] Sopena C, Diéguez PM, Sáinz D, Urroz JC, et al. Conversion of a commercial spark ignition engine to run on hydrogen: performance comparison using hydrogen and gasoline. Int J Hydrogen Energy 2010;35:1420–9. https://doi.org/10.1016/j.ijhydene.2009.11.090.
[10] Verhelst S, Maesschalck P, Rombaut N, Sierens R. Increasing the power output of hydrogen internal combustion engines by means of supercharging and exhaust gas recirculation. Int J Hydrogen Energy 2009;34:4406–12. https://doi.org/10.1016/j.ijhydene.2009.03.037.
[11] Verhelst S, De Landtsheere J, De Smet F, Billiouw C, et al. Effects of supercharging, EGR and variable valve timing on power and emissions of hydrogen internal combustion engines. SAE Int. J. Engines 2009;1(1):647–56. https://doi.org/10.4271/2008-01-1033.
[12] Yang Z, Zhang F, Wang L, Wang K, et al. Effects of injection mode on the mixture formation and combustion performance of the hydrogen internal combustion engine. Energy 2018;147:715–28. https://doi.org/10.1016/j.energy.2018.01.068.
[13] Berckmüller M, Rottengruber H, Eder A, Brehm N, et al. Potentials of a charged SI-hydrogen engine. SAE technical paper 2003-01-3210. 2003. https://doi.org/10.4271/2003-01-3210.
[14] Eichlseder H, Wallner T, Freymann R, Ringler J. The potential of hydrogen internal combustion engines in a future mobility scenario. SAE technical paper 2003-01-2267. 2003. https://doi.org/10.4271/2003-01-2267.
[15] Hamada KI, Rahman MM, Abdullah MA, Bakar RA, et al. Effect of mixture strength and injection timing on combustion characteristics of a direct injection hydrogen-fueled engine. Int J Hydrogen Energy 2013;38:3793–801. https://doi.org/10.1016/j.ijhydene.2013.01.092.
[16] Mohammadi A, Shioji M, Nakai Y, Ishikura W, et al. Performance and combustion characteristics of a direct injection SI hydrogen engine. Int J Hydrogen Energy 2007;32:296–304. https://doi.org/10.1016/j.ijhydene.2006.06.005.
[17] Wimmer A, Wallner T, Ringler J, Gerbig F. H2-Direct injection – a highly promising combustion concept. SAE technical paper 2005-01-0108. 2005. https://doi.org/10.4271/2005-01-0108.
[18] Yun H, Bu Z, Yang Z, Wang L, et al. Optimization of fuel injection timing and ignition timing of hydrogen fueled SI engine based on DOE-MPGA. Int J Hydrogen Energy 2023;48:9462–73. https://doi.org/10.1016/j.ijhydene.2022.12.068.

[19] Matthias N, Wallner T, Scarcelli R. A hydrogen direct injection engine concept that exceeds U.S. DOE light-duty efficiency targets. SAE Int. J. Engines 2012;5(3):838–49. https://doi.org/10.4271/2012-01-0653.
[20] Salazar V, Kaiser S. Interaction of intake-induced flow and injection jet in a direct-injection hydrogen-fueled engine measured by PIV. SAE technical paper 2011-01-0673. 2011. https://doi.org/10.4271/2011-01-0673.
[21] Salazar V, Kaiser S. An optical study of mixture preparation in a hydrogen-fueled engine with direct injection using different nozzle designs. SAE Int. J. Engines 2010;2(2):119–31. https://doi.org/10.4271/2009-01-2682.
[22] Scarcelli R, Wallner T, Matthias N, Salazar V, et al. Mixture Formation in direct injection hydrogen engines: CFD and optical analysis of single- and multi-hole nozzles. SAE Int. J. Engines 2011;4(2):2361–75. https://doi.org/10.4271/2011-24-0096.
[23] Fu Z, Gao W, Li Y, Hua X, et al. Numerical simulation of the mixture distribution and its influence on the performance of a hydrogen direct injection engine under an ultra-lean mixture condition. Int J Hydrogen Energy 2023;48:19700–12. https://doi.org/10.1016/j.ijhydene.2023.02.041.
[24] Gammaidoni T, Miliozzi A, Zembi J, Battistoni M. Hydrogen mixing and combustion in an SI internal combustion engine: CFD evaluation of premixed and DI strategies. Case Stud Therm Eng 2024;55:104072. https://doi.org/10.1016/j.csite.2024.104072.
[25] Piano A, Puccillo F, Millo F, Giordana S, et al. Experimental investigation on the optimal injection and combustion phasing for a direct injection hydrogen-fuelled internal combustion engine for heavy-duty applications. Int J Hydrogen Energy 2025;100:398–406. https://doi.org/10.1016/j.ijhydene.2024.12.194.
[26] Laget O, Rouleau L, Cordier M, Duffour F, et al. A comprehensive study for the identification of the requirements for an optimal H2 combustion engine. Int J Engine Res 2023;24:4326–42. https://doi.org/10.1177/146808742311676.
[27] Sfriso S, Berni F, Fontanesi S, d'Adamo A, et al. Combination of G-Equation and Detailed Chemistry: an application to 3D-CFD hydrogen combustion simulations to predict NOx emissions in reciprocating internal combustion engines. Int J Hydrogen Energy 2024;89:161–76. https://doi.org/10.1016/j.ijhydene.2024.09.252.
[28] Mortellaro F. S., Silvestri N., Zaffino F., Medda M., et al., "Effect of start of injection in a hydrogen-fueled DISI engine: experimental and numerical investigation," SAE Technical paper 2023-24-0015, doi: 10.4271/2023-24-0015.
[29] Medda M, Calia V, Di Sacco M, Gullino F, et al. Challenges and opportunities in developing a hydrogen high specific power SCE in the roadmap towards zero net GHG. 32nd aachen colloquium sustainable mobility. 2023. https://oevk.at/en/papers.
[30] Leick P, Jochmann P, Geiler j, Stapf K, et al. Analysis of fuel injection and mixture formation in hydrogen engines. 2023.
[31] Paltrinieri S, Olcuire M, Calia V, Mortellaro F, et al. Experimental and numerical investigation of hydrogen injection and its preliminary impact on high performance engines development. SAE technical paper 2023-01-0402. 2023. https://doi.org/10.4271/2023-01-0402.
[32] Xinyu L, Yang L, Chan Q, Kook S. Split injection strategies for a high-pressure hydrogen direct injection in a small-bore dual-fuel diesel engine. Int J Hydrogen Energy 2024;57:904–17. https://doi.org/10.1016/j.ijhydene.2024.01.065.
[33] Scalambro A, Piano A, Millo F, Scinicariello N, et al. Numerical analysis of the hydrogen-air mixture formation process in a direct-injection engine for off-road applications. Int J Hydrogen Energy 2024;77:1286–95. https://doi.org/10.1016/j.ijhydene.2024.06.193.
[34] Akar F, Ozener O. Numerical investigation of in-cylinder gas motion dynamics in a heavy-duty direct injection hydrogen internal combustion engine. Int J Hydrogen Energy 2024;86:730–41. https://doi.org/10.1016/j.ijhydene.2024.08.338.
[35] Chen W, Lu C, Zuo Q, Kou C, et al. Combustion characteristics analysis and performance evaluation of a hydrogen engine under direct injection plus lean burn mode. J Clean Prod 2024;470:143323. https://doi.org/10.1016/j.jclepro.2024.143323.
[36] Mortellaro F, Tonelli R, Medda M. Ultra-lean mixture formation and combustion of a hydrogen-fuelled high-performance DI-SI engine: an experimental and numerical study. In: Conference proceeding at THIESEL; 2024. https://doi.org/10.4995/Thiesel.2024.679601. 10-13 September 2024 at Valencia.
[37] Kaczmarczyk K. O., Liu X., Im H. G., Turner J., et al., "Investigation of URANS CFD methods for supersonic hydrogen jets," SAE Technical paper 2024-01-2687, doi: 10.4271/2024-01-2687.
[38] Anaclerio G, Capurso T, Torresi M, Camporeale SM. Numerical characterization of hydrogen under-expanded jets with a focus on Internal Combustion Engines applications. Int J Engine Res 2023;24:3342–58. https://doi.org/10.1177/14680874221148789.
[39] Postrioti L, Mariani F, Battistoni M. Experimental and numerical momentum flux evaluation of high pressure Diesel spray. Fuel 2023;98:149–63. https://doi.org/10.1016/j.fuel.2012.03.043.
[40] Wu B, Torelli R, Pei Y. Numerical modeling of hydrogen mixing in a direct-injection engine fueled with gaseous hydrogen. Fuel 2023;341:127725. https://doi.org/10.1016/j.fuel.2023.127725.
[41] Addepalli SK, Pei Y, Zhang Y, Scarcelli R. Multi-dimensional modeling of mixture preparation in a direct injection engine fueled with gaseous hydrogen. Int J Hydrogen Energy 2022;47:29085–101. https://doi.org/10.1016/j.ijhydene.2022.06.182.
[42] Hamzehloo A, Aleiferis P. Computational study of hydrogen direct injection for internal combustion engines. SAE technical paper 2013-01-2524. 2013. https://doi.org/10.4271/2013-01-2524.
[43] Iaccarino S, Breda S, D'Adamo A, Fontanesi S, et al. Numerical simulation and flame analysis of combustion and knock in a DISI optically accessible Research engine. SAE Int. J. Engines 2017;10(2):576–92. https://doi.org/10.4271/2017-01-0555.
[44] Soave G. Equilibrium constants from a modified Redkh-Kwong equation of state. Chem Eng Sci 1972;27:1197–203. https://doi.org/10.1016/0009-2509(72)80096-4.
[45] Coratella C, Tinchon A, Oung R, Doradoux L, et al. Experimental characterization of a hydrogen hollow cone jet at under-expanded conditions via schlieren technique. Int J Hydrogen Energy 2024;72:730–43. https://doi.org/10.1016/j.ijhydene.2024.05.411.
[46] Tang Meng. Spray and combustion studies of high reactivity gasoline in comparison to diesel under advanced compression ignition engine conditions. Open access dissertation. Michigan Technological University; 2018. https://doi.org/10.37099/mtu.dc.etdr/686.
[47] Cabezas K. M., Zaihi A., Liu X., Aljohani B., et al., "Numerical analysis of different hydrogen injector characteristics in a constant volume chamber," SAE technical paper 2024-01-2693, doi:10.4271/2024-01-2693.
[48] Colin O, Benkenida A, Angelberger C. 3D modeling of mixing, ignition and combustion phenomena in highly stratified gasoline engines. Oil & Gas Science and Technology - Rev. IFP 2003;58(1):47–62.
[49] D'Adamo A, Breda S, Fontanesi S, Cantore G. A RANS-based CFD model to predict the statistical occurrence of knock in spark-ignition engines. SAE Int. J. Engines 2016;9(1):618–30. https://doi.org/10.4271/2016-01-0581.
[50] Piano A, Rolando L, Roggio S, Millo F, et al. Experimental and numerical investigation of abnormal combustion phenomena in high-performance hydrogen direct-injection engine operated in stochiometric conditions. Int J Engine Res 2025;0(0). https://doi.org/10.1177/14680874241302562.
[51] Sun W, Zhao Q, Curran HJ, Deng F, et al. Further insights into the core mechanism of H2/CO/NOx reaction system. Combust Flame 2022;245:112308. https://doi.org/10.1016/j.combustflame.2022.112308.
[52] Olm C, Zsély IG, Palvolgy R, Varga T, et al. Comparison of the performance of several recent hydrogen combustion mechanisms. Combust Flame 2014;161:2219–34. https://doi.org/10.1016/j.combustflame.2014.03.006.
[53] Ribnishki A., Charles C., Esposito S., Akehurst S., et al., "Comparison of the predictive capabilities of chemical kinetic models for hydrogen combustion applications," SAE technical papers, 2024-01-2116, doi:10.4271/2024-01-2116.
[54] Baudone A. D., Madia M., Pavan N., Cordisco I., et al., "Chemical kinetics calculation of H2 Laminar Flame Speed: assessment of the performance of public available mechanisms at engine relevant conditions," J Phys Conf, Volume 2893, The 79th ATI Annual Congress 04/09/2024 - 06/09/2024 Genoa, Italy, doi: 10.1088/1742-6596/2893/1/012094.
[55] Colin O, Truffin K. A spark ignition model for large eddy simulation based on an FSD transport equation (ISSIM-LES). Proc Combust Inst 2011;33:3097–104. https://doi.org/10.1016/j.proci.2010.07.023.
[56] Berni F, Cicalese G, Borghi M, Fontanesi S. Towards grid-independent 3D-CFD wall-function-based heat transfer models for complex industrial flows with focus on in-cylinder simulations. Appl Therm Eng 2021;190:116838. https://doi.org/10.1016/j.applthermaleng.2021.116838.
[57] Berni F, Cicalese G, Sparacino S, Cantore G. On the existence of universal wall functions in in-cylinder simulations using a low-Reynolds RANS turbulence model. In: AIP conference proceedings. American Institute of Physics Inc.; Dec. 2019. https://doi.org/10.1063/1.5138752.
[58] Berni F, Fontanesi S. A 3D-CFD methodology to investigate boundary layers and assess the applicability of wall functions in actual industrial problems: a focus on in-cylinder simulations. Appl Therm Eng 2020;174:115320. https://doi.org/10.1016/j.applthermaleng.2020.115320.
[59] Jennings MJ, Jeske FR. Analysis of the injection process in direct injected natural gas engines: Part II—effects of injector and combustion chamber design. J Eng Gas Turbines Power Oct. 1994;116(4):806–13. https://doi.org/10.1115/1.2906889.